

# ~~Modelling Fire Ignition and Suppression in INFERNO: A~~ ~~Socio-Economic Approach Based on~~ Assessing the Impact of the Human Development Index on Historical Trends in the INFERNO Fire Model

João C. M. Teixeira<sup>1,2,4</sup>, Chantelle Burton<sup>1</sup>, Douglas I. Kelley<sup>3</sup>, Gerd A. Folberth<sup>1</sup>, Fiona M. O'Connor<sup>1,2</sup>, Richard A. Betts<sup>1,2</sup>, and Apostolos Voulgarakis<sup>4,5</sup>

<sup>1</sup>Met Office, Fitzroy Road, EX1 3PB, Exeter, UK

<sup>2</sup>Global Systems Institute, Department of Mathematics & Statistics, University of Exeter, EX4 4QE, UK

<sup>3</sup>UK Centre for Ecology and Hydrology, Wallingford OX10 8BB, U.K

<sup>4</sup>Leverhulme Centre for Wildfires, Environment and Society, Department of Physics, Imperial College London, London, UK

<sup>5</sup>School of Environmental Engineering, Technical University of Crete, Chania, Greece

**Correspondence:** João C. M. Teixeira (joao.teixeira@metoffice.gov.uk)

**Abstract.** Earth System Models (~~ESM~~), ~~have struggled to reproduce the historical decline~~ ESMs capture long-term historical trends in burnt area, ~~with discrepancies largely attributed to the under-representation of~~ but they struggle to reproduce the pronounced decline observed over the past two decades, largely because anthropogenic fire suppression and related socio-economic influences are not adequately represented. Key factors such as agricultural expansion, land-use changes, fire management policies, and landscape fragmentation have all contributed to reduced fire activity, especially in tropical savannas, but these are not adequately captured in the fire model ~~formulation that underpins~~ formulations that underpin most ESMs.

This study investigates whether the observed downward trend in global burnt area during the period 1998–2016 can be better represented in the JULES-INFERNO fire model by incorporating a simplified representation of direct human impacts on fire. Specifically, we focus on the Human Development Index (HDI), which reflects socio-economic development and, in turn, influences fire suppression efforts. By ~~incorporating~~ implementing globally uniform assumption that anthropogenic fire ignitions and suppression decline linearly with HDI into INFERNO, we aim to improve the representation of fire ignition and suppression dynamics. ~~Results show that including HDI-driven~~

Including HDI-based socio-economic factors ~~reduces~~ substantially reduces regional biases in annual ~~burnt area, particularly in~~ burned area. In Temperate North America, for example, model bias decreases from +735.57 % to +44.46 %, with similarly large reductions in Central America, ~~and Europe. While including HDI corrects regional biases, it also introduces a global negative bias as compensating errors at the regional level are addressed. Overall, this approach~~ Southern Hemisphere South America, Europe, and the Middle East. HDI also improves the representation of ~~burnt~~ burned area trends in eight ~~out of of the~~ 14 regions, ~~including Southern Hemisphere South America and Northern Hemisphere Africa, where observations show negative trends. Despite mixed results in other fire regions, this study demonstrates that incorporating a~~ GFED4s regions that exhibit significant negative trends in observations. However, correcting large positive regional biases removes compensating

errors in the original configuration, resulting in a stronger global negative bias, shifting from -34.35 Mha to approximately -111 Mha.

While HDI enhances regional performance and better captures recent downward trends in some areas, it introduces trade-offs, including dampened interannual variability and underestimation of medium to large fire events. Overall, incorporating HDI offers a computationally efficient way to represent socio-economic dimension in INFERNO through HDI provides a simple and effective way to improve fire model performance. It also enhances the ability of ESMs to capture human-environment interactions and offering valuable insights for future climate modelling and fire management strategies influences within INFERNO. Nevertheless, the linear and spatially uniform implementation remains a first-order approximation and cannot fully capture the complex regional, cultural, and policy-driven dynamics shaping human–fire interactions.

## 30 1 Introduction

Globally, burnt area trends are influenced by complex interactions between climate change, human activities, and natural ecosystem processes, resulting in large climate change and variability over the past few decades. However, the long-term trend (e.g., 1997 - 2016) has shown an overall decline in global burnt area, especially driven by changes in burnt area of African savannas and grasslands (decline of 1.27 % per year (Andela et al., 2017)). The trend, shown in Figure 1 b), is attributed to changes in land use, particularly agricultural expansion and intensification in savanna and grassland regions, which reduces the availability of fuel for fires (Riley et al., 2019; Andela et al., 2017).

In addition, fire is also actively used as a land management tool, for example to clear land for agriculture, manage vegetation, and maintain pasture systems, particularly in tropical and subtropical landscapes.

Figure 1 illustrates the broad-scale spatial patterns and long-term trends of burnt area, fire weather, and the Human Development Index (HDI).

Climate is a key factor that also influences fire activity (Archibald et al., 2010; Andela et al., 2017; Jones et al., 2022; Kelley et al., 2019). Rising temperatures are leading to longer fire seasons, particularly in temperate and boreal regions (Sullivan et al., 2022; Jones et al., 2024). Additionally, reduced rainfall during the critical phase of fire seasons increases the likelihood of large-scale fires, while increased rainfall during certain times of the year can promote vegetation growth, providing more fuel for future fires. However, while climate strongly influences inter-annual variability and is increasingly important for long-term trends, particularly in temperate and boreal regions, human activity—such as land use change, agricultural expansion, and active fire suppression—has been the dominant driver of long-term declines in global burnt area, especially in tropical savannas (Riley et al., 2019; Andela et al., 2017)(Riley et al., 2019; Andela et al., 2017; Marlon et al., 2008).

Furthermore, human population density and prosperity can significantly impact burnt areas. (Andela et al., 2017) show that due to population growth, socioeconomic development, and the increased demand for agricultural products in regional and global markets, there has been a shift towards more capital-intensive agriculture, resulting in fewer and smaller fires. These factors have a predictable impact on the use of fire, with a strong inverse correlation between the area burned and economic development.

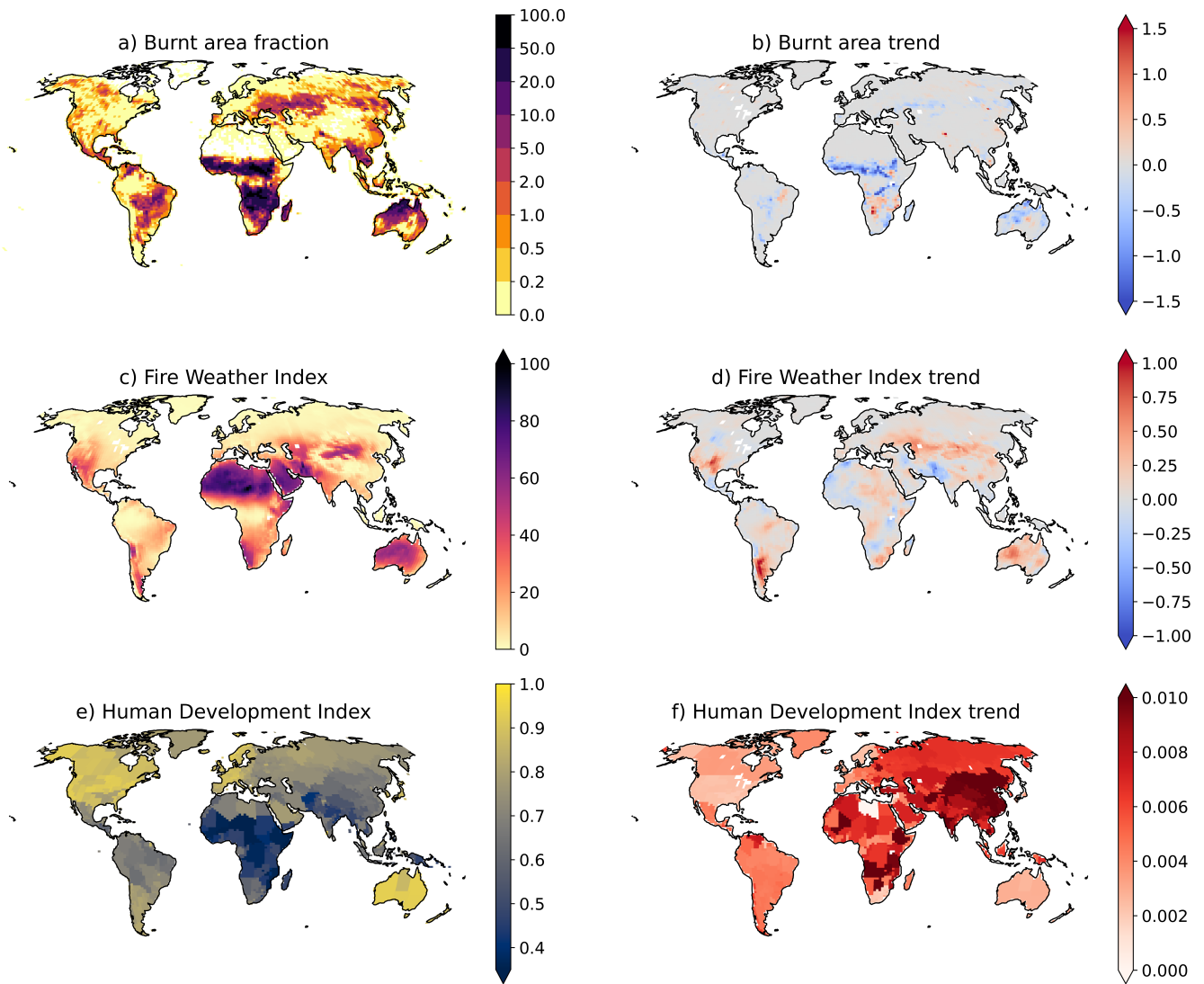


**Figure 1.** Global distribution of a) Burnt area fraction from the Global Fire Emission Database version 4 (GFED4s) (%) total annual average (1997 - 2016) and b) respective trend ( $\% \text{ year}^{-1}$ ); c) Fire Weather Index average (FWI) average across 1997 - 2016 and d) respective trend ( $\text{year}^{-1}$ ); e) Human Development Index average (HDI) average across 1997 - 2016 and f) respective trend ( $\text{year}^{-1}$ ). The FWI maps represent long-term climatological averages intended to illustrate broad-scale spatial patterns and trends in fire-conducive conditions.

55 In Coupled Model Intercomparison Project frameworks, fire processes are generally represented through simplified, global-scale schemes that link burned area to vegetation, fuel availability, and climate conditions. Most models include ignition from lightning and human sources, with fire spread and, flammability, and fuel continuity. These schemes capture broad spatio-temporal patterns of fire but tend to not resolve fine-scale processes such as local suppression, management practices, or sub-grid fuel heterogeneity (Yue et al., 2014; Rabin et al., 2017).

The study by Li et al. (2024) shows that the Earth System Models (ESMs) used to provide state-of-the-art climate projections for Phase 6 of the Coupled Model ~~intercomparison~~ Intercomparison Project (CMIP6; Eyring et al. (2016)) ~~fail to reproduce the do not reproduce the observed~~ decline in global burned area and fire carbon emissions ~~observed~~ over the past two decades. ~~They~~ They identify the primary ~~reason for cause of~~ this discrepancy as an underestimation of anthropogenic fire suppression in ~~fire models~~. Key fire-enabled models (mathematical representation of a real-world system). This finding is consistent with the data-driven analysis of Forkel et al. (2019), who quantitatively disentangled the relative contributions of climate and human drivers of fire activity and demonstrated there is a strong sensitivity to climate variables, vegetation properties, and to socio-economic variables.

Moreover, ~~key~~ key human-driven factors—~~such as agricultural expansion, land-use changes~~ change, fire management policies, and landscape fragmentation—~~have significantly~~, have substantially reduced fire activity, particularly in tropical savannas (~~Andela et al., 2017~~)(Andela et al., 2017; Forkel et al., 2019). However, most CMIP6 models do not adequately ~~account for~~ represent these suppression mechanisms, ~~resulting in leading to~~ an overestimation of burned area ~~and trends and associated~~ fire-related carbon emissions.

Most global fire models, such as JULES-INFERNO (Mangeon et al., 2016; Burton et al., 2019), apply simplistic representations of human ignitions, generally specified as a function of population density, increasing up to a threshold value after which there are no additional ignitions with an increasing population (Rabin et al., 2017; Teckentrup et al., 2019; Ford et al., 2021). This approach does not account for the impacts of socio-economic factors on anthropogenic fire ignitions or suppression. It also does not capture how humans influence regional variation in contemporary burning practices.

This misrepresentation has important implications for climate projections and carbon cycle modelling, and emphasizes the need for better integration of dynamic human influences on fire regimes, such as incorporating evolving socio-economic factors (e.g., population growth, infrastructure expansion, and fire suppression strategies) into fire models (Li et al., 2024).

80 ~~The Human Development Index (HDI)~~ In current global fire models, changes in fire activity are typically quantified through a separation of climate-driven controls—such as fire weather, fuel moisture, and vegetation productivity—from anthropogenic influences, which are commonly represented using simplified proxies such as population density or land-use change. As shown by (Burton et al., 2024), this structural separation strongly shapes how models attribute historical and future changes in fire activity to climate versus human drivers, and can lead to substantial differences in simulated fire responses when anthropogenic processes are under-represented.

85 Accurately simulating fire is also essential for reliable climate projections, as fire and climate are coupled through two-way feedbacks. Fire activity influences atmospheric composition, surface albedo, and land-carbon exchanges, while climate change alters fire weather, fuel availability, and ignition conditions. Recent work by (Verjans et al., 2025) highlights the importance of

these fire–climate feedbacks, showing that improved fire representations can substantially affect simulated climate responses.

90 This further underscores the need for realistic fire modelling within ESMs.

HDI is a composite measure that combines four key metrics: life expectancy at birth, expected years of schooling, average years of schooling, and Gross National Income (GNI) per capita (Bhanojirao, 1991). These metrics are normalized by their respective maximum values, and the HDI is calculated as the geometric mean of life expectancy, education, and GNI per capita. The HDI has been used in various studies to better understand ~~the socio-economic impacts-influences~~ on the Earth System(ES) (Türe, 2013; Hiekel, 2020; Roy et al., 2023), including links between development and environmental pressure (Türe, 2013), the decoupling between human development and resource use or emissions (Hiekel, 2020), and the role of socio-economic development pathways in shaping sustainability outcomes at regional and global scales (Roy et al., 2023).

Chuvieco et al. (2021) demonstrates that the HDI is strongly correlated with ~~the~~ inter-annual variability ~~in-of~~ burned area. Chuvieco et al. (2021) shows that higher HDI is associated with lower fire activity, driven by reduced dependence on fire for agricultural purposes due to ~~Regions with higher HDI show lower variability, largely because~~ increased mechanization and a shift away from agrarian livelihoods ~~.In contrast, regions reduce the need for fire in agricultural practices. Conversely, areas~~ with lower HDI exhibit ~~more consistent fire activity~~ greater variability, reflecting continued reliance on fire as a land management tool. ~~The study also demonstrated that incorporating~~ Incorporating socio-economic indicators ~~like such as~~ HDI into fire models significantly ~~improves-enhances~~ their ability to reproduce observed patterns of fire-variability.

105 More recently, Perkins et al. (2024) introduced WHAM! (the Wildfire Human Agency Model), a global behavioural, geospatial model designed to represent human fire use and management in a form that can be coupled to dynamic global vegetation models, demonstrated via coupling with JULES-INFERNO. WHAM! is empirically grounded in a global synthesis of anthropogenic fire impacts and seeks to move beyond single-proxy parametrisations by representing underlying behavioural and land-system drivers that shape how people ignite, manage, and suppress fires across regions. As such, WHAM! constitutes a more sophisticated, process-oriented attempt to incorporate anthropogenic drivers in fire modelling. In contrast, the HDI-based implementation in this work is intentionally simplified to remain tractable for ESM applications.

115 Additionally, Li et al. (2013) and Zou et al. (2019) investigated the use of Gross Domestic Product (GDP) to parametrise human influences on ~~fires. However, their approach was limited to agricultural fires and did not account for broader human factors in fire management~~ fire activity. While these approaches capture broad relationships between economic development and fire occurrence, they offer a limited representation of the underlying socio-economic processes that govern fire ignition and suppression.

120 Human influences on fire activity have become ~~more-increasingly~~ pronounced since the late 18<sup>th</sup> century, ~~reflecting the effects-of~~ driven by industrialization, climate change, land clearance, population growth, the ~~replacement-decline~~ of traditional fire management practices, and the ~~development-emergence~~ of large-scale firefighting and fuel management in the 20<sup>th</sup> century (Bowman et al., 2020). ~~This demonstrated~~ These trends highlight the need for improved data collection to ~~better-accurately~~ quantify and model ~~fire activity and human populations, including their~~ the relationships between human populations and fire activity, including factors such as socio-economic status ~~and~~, historical, cultural, and political legacies. ~~As vegetation fires’~~ Understanding these interactions is particularly important as the economic and environmental impacts ~~are likely to worsen due~~

~~to~~ of vegetation fires are expected to intensify under anthropogenic climate change (Sullivan et al., 2022; Jones et al., 2024; Haas et al., 2024), this is increasingly urgent. Additionally, Nikolakis and Roberts (2022) examined how policy learning occurs in wildfire governance, focusing on how wildfire policies in British Columbia have evolved. Their case study shows that policy transfer from similar contexts, particularly Indigenous peoples and their governments, can reshape perceptions of wildfire risk and solutions as we adapt to an uncertain future. Similarly, Pandey et al. (2023) explored the complexity of socio-economic factors on fire and the varied fire management policies worldwide, demonstrating that despite differences, these policies have led to a gradual reduction in fire occurrences and burned area over time.

Several studies ~~have shown that~~ indicate that, in developed regions, ~~land and fire management policies play a more significant role in controlling fire ignitions than other human behaviours~~ (Nikolakis and Roberts, 2022; Jacobson et al., 2022; Ford et al., 2021; Curt and Frejaville, 2018). ~~fire occurrence and impacts are strongly shaped by governance and policy, rather than individual behaviour alone. For example, changes in policy and governance have been shown to influence fire outcomes~~ (Nikolakis and Roberts, 2022), while risk framing and coordination efforts also play an important role (Jacobson et al., 2022). Modelling approaches that emphasise management institutions further highlight the significance of governance in shaping fire dynamics (Ford et al., 2021). Observed reductions in fire numbers or size following prevention and suppression policy shifts provide additional empirical support (Curt and Frejaville, 2018), and studies demonstrate that policy design and its dependence on local stakeholder and contextual factors can determine effectiveness (Carreiras et al., 2014). Finally, institutional capacity and spending have been linked directly to fire outcomes, underscoring the importance of resources and coordination (Mourão and Martinho, 2014).

Notably, Curt and Frejaville (2018) found that wildfire policies in Mediterranean France have led to a nearly linear decrease in the number of fires since 1975, though the burnt area has fluctuated more abruptly. Therefore, representing land and fire management policies in global fire models is crucial to building confidence in the modelling frameworks which are used to understand future climate regimes. This, in turn, can underpin decision-making by policy-makers in regards to fire policy in the future.

Nonetheless, how socio-economic factors impact on fires is complex and dependent on many factors that are difficult to represent in an ESM context. These factors depend on policies implemented at government level, as well as cultural behaviour which varies widely across the world. As a result, the formulation of Climate and ~~ES models~~ ESMs does not allow for representing these details.

Rather than attempting to capture the full complexity of socio-economic influences on fire, this study explores a simplified, emergent relationship ~~—~~ using HDI as a proxy ~~—~~, that is better suited for large-scale applications. Here, fire suppression is used broadly to represent human actions that limit fire spread, including active containment and land management practices, whose implementation and effectiveness vary regionally with resources and infrastructure. Processes such as fine-scale suppression tactics, planned burns, fuel management, and weather-driven fire extinction are not explicitly represented. We use observed datasets of HDI, burnt area, and ~~fire weather index~~ Fire Weather Index (FWI) to derive a relationship between HDI and burnt area, and ~~and~~ model data to ~~devise an approach to implement these~~ implement this approach in the INFERNO fire model. ~~A detailed description of the observed datasets is provided in the Appendix, section 2.1.~~

In Section 2, we explore the relation between HDI and burnt area and describe the INFERNO fire model, the coupling of INFERNO to the latest representation of the land surface model (JULES-ES) as used in the UK’s Earth System Model (UKESM1), and how we include HDI into INFERNO’s ignition scheme. In Section 3, we evaluate the impact of considering HDI on burnt area, burnt area trends, as well as the impact of external model drivers of burnt area trends. Discussion and conclusions from this work are presented in Section 4, where we focus on novel model results, placing the link between socio-economic factors and fires in context with existing literature. Model limitations and known issues are also highlighted.

## 2 Methods

### 2.1 Observed Datasets

#### 2.1.1 The Human Development Index dataset

HDI originated from the annual Human Development Reports created by the United Nations Development Programme (UNDP) Human Development Report Office. These reports had the explicit purpose of shifting the focus of development economics from national income accounting to people-centred policies. The aim was to provide a simple composite measure of human development to convince the public, academics, and politicians to evaluate development not only by economic advances but also improvements in human well-being. HDI serves as a crucial metric for assessing the development status of regions globally, and it has been used in several studies to better understand the socio-economics impacts in the Earth System (ES) (Türe, 2013; Hickel, 2020; Roy et al., 2023).

HDI is a composite index (ranging from zero to one) measuring four key metrics (Bhanojirao, 1991):

- life expectancy at birth
- expected years of schooling
- average years of schooling
- gross national income (GNI) per capita

These metrics are then normalised by their respective maximum value, and HDI is calculated as the geometric mean of life expectancy, education, and GNI per capita, as shown in Eq. 1.

$$HDI = (H_N \cdot E_N \cdot I_N)^{\frac{1}{3}} \quad (1)$$

where  $H_N$  is the normalised life expectancy,  $E_N$  is the normalised arithmetic mean of the two education indices and  $I_N$  is the normalised GNI.

The work conducted by Kummu et al. (2018) introduces gridded global datasets for Gross Domestic Product (GDP) and Human Development Index (HDI), covering a 25-year period from 1990 to 2015 with annual frequency and a spatial resolution

of 5 arc-minutes. This temporal coverage and high-resolution global scope enable comprehensive analyses of trends, patterns, and changes in HDI across diverse regions and timescales.

190 To produce these datasets, Kummu et al. (2018)s employed a comprehensive approach. For GDP, they utilized both sub-national and national-level data sources. Sub-national GDP data was derived from previous research, while national-level data was sourced from reputable institutions such as the World Bank and the Central Intelligence Agency World Factbook. The HDI dataset was compiled by initially constructing a full national HDI dataset based on data from the Human Development Reports by UNDP. For countries not included in the UNDP reports, independent data sources were utilized, and for missing or outdated data, a methodology involving scaled regional data was adopted.

### 2.1.2 Burnt Area observation

195 Global Fire Emission Database version 4 (GFED4s) is a long-running, operationally updated dataset used globally for fire and emissions research. While the core methodological reference (Giglio et al., 2013) describes the development of the GFED4s framework, the dataset itself has been continuously updated to include fire emissions up to recent years (e.g., including 1997–2016).

200 We use data from the GFED4s to understand the relation between HDI and burnt area, as well as to assess the model performance in simulating burnt area. This dataset is provided as a gridded product at a  $0.25^\circ$  resolution. It is derived from a multi-sensor satellite dataset, including satellite data based on active fire detection, and including small fires based on statistical modelling, as detailed in (Randerson et al., 2012).

We apply regions defined in the GFED4s dataset to the modelled data to evaluate the results at a regional level (Figure A1).

### 2.1.3 Fire Weather Index

205 The Canadian FWI is a component of the Canadian Forest Fire Danger Rating System (CFFDRS) and provides a numerical rating of fire intensity based solely on weather conditions (temperature, relative humidity, wind speed, and precipitation). Although it was originally developed for Canadian boreal forest conditions, the FWI system is not region-specific and has been successfully applied in diverse ecosystems worldwide, including in Europe, South America, Australia, and parts of Africa and Asia. Its broad adoption stems from its simplicity, weather-based formulation, and scalability (Field et al., 2015).

210 The work developed by Vitolo et al. (2020) provides an ERA5-based global meteorological wildfire danger dataset based on the Global ECMWF Fire Forecast (GEFF) model and the ERA5 reanalysis.

In this dataset the FWI is calculated using meteorological variables (e.g., such as temperature, humidity, precipitation, and wind speed) driven by the ERA5 reanalysis dataset. To accurately represent wildfire conditions at local noon, when fire danger is typically highest, atmospheric fields from ERA5 undergo preprocessing, stitching together hourly forecasts, ensuring that meteorological conditions are representative of 12:00 noon local time around the world.

215 The GEFF model, calculates the FWI by modelling fuel moisture response to atmospheric forces at different depths. Three fuel moisture levels are used, representing surface fuels, deeper organic material, and compact fuels, each responding at

different rates to changes in weather. These moisture codes are then combined to estimate fire behaviour, such as the rate of spread and fire intensity, providing a comprehensive fire danger index.

220 The GEF-ERA5 FWI reanalysis dataset, available from 1979 onwards at a spatial resolution of 28 km, was used in this study with monthly averaged values.

When comparing datasets (modelled or observed) at different grid resolutions, the higher-resolution dataset is re-gridded to the lowest-resolution grid using a first-order conservative area-weighted re-gridding method.

## 2.2 Relation between HDI and Burnt Area

225 As climate is a dominant factor influencing fire activity, it is essential to first account for and remove climate change's influence before exploring the effects of socio-economic factors on burnt area. For this, and considering that the ~~Fire Weather Index (FWI)~~ FWI depends solely on the weather variables that drive fire activity, we ~~apply a linear regression model to the FWI data, and the predicted slope from this linear regression model is then~~ perform a deweathering procedure at each individual grid cell.

230 For each grid cell  $(i, j)$ , we consider the monthly time series  $(t)$  of normalised FWI,  $FWI_{i,j}(t)$ , and normalised burnt area,  $BA_{i,j}(t)$ , over the study period. A linear regression of the FWI time series is fitted to estimate the local climate-driven trend,  $\beta_{i,j}^{FWI}$ , while independently a linear regression of the burnt area time series is used to estimate its intercept,  $\alpha_{i,j}^{BA}$ .

The climate-driven component of burnt area is then estimated as

$$\widehat{BA}_{i,j}(t) = \beta_{i,j}^{FWI} t + \alpha_{i,j}^{BA} \quad (2)$$

235 Finally, the climate-driven component is removed from the normalised ~~values of burnt area~~. A burnt area time series while preserving the original mean:

$$BA_{i,j}^*(t) = BA_{i,j}(t) - \widehat{BA}_{i,j}(t) + \overline{BA}_{i,j}, \quad (3)$$

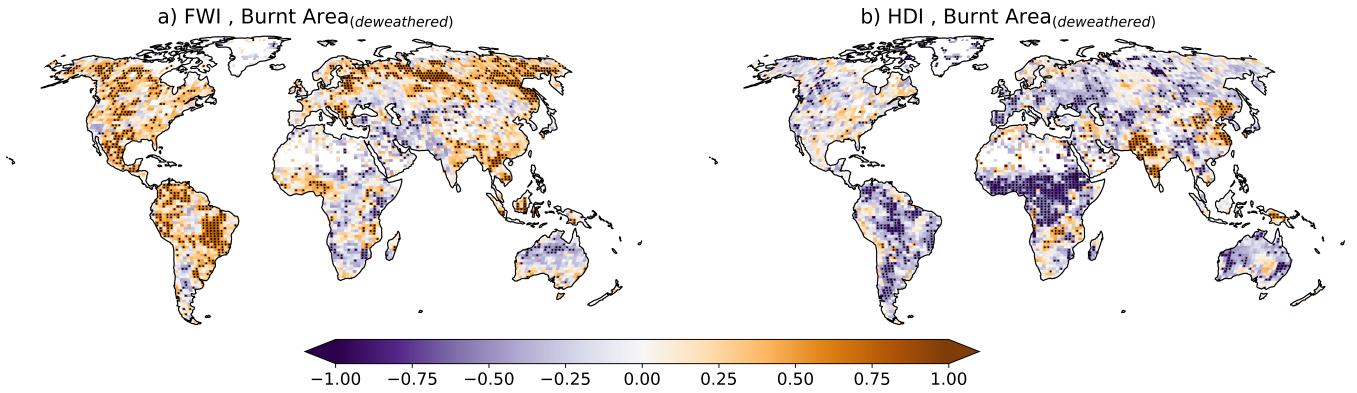
where  $\overline{BA}_{i,j} = \frac{1}{T} \sum_{t=1}^T \widehat{BA}_{i,j}(t)$  is the temporal mean of the estimated climate-driven component at each grid cell.

240 This results in a normalised burnt area dataset ~~is produced with where~~ the influence of ~~climate removed fire-weather variability has been minimized~~ (deweathered), ~~and which is then~~ used to analyse how socio-economic factors, through the ~~use of~~ HDI, impact fire activity.

In this analysis, we make the simplifying assumption that, once the influence of weather is removed, residual variations or trends in burnt area can be primarily attributed to socioeconomic factors. We note, however, that fuel availability and continuity can also be important determinants of fire activity and may influence burnt area trends even after deweathering.

245 To ensure consistency across our burnt area results, we define the burnt area fraction as the proportion of each grid cell that burns in a given year, calculated as the burned area divided by the total cell area (Giglio et al., 2013).

Figure 2 shows the spatial correlation coefficient between FWI and deweathered burnt area (panel a) and between HDI and deweathered burnt area (panel b). ~~Although the spatial correlation coefficient between FWI, HDI, and the~~ While these correlations are spatially variable, over most of the globe the correlation between deweathered burnt area ~~are spatially varied~~



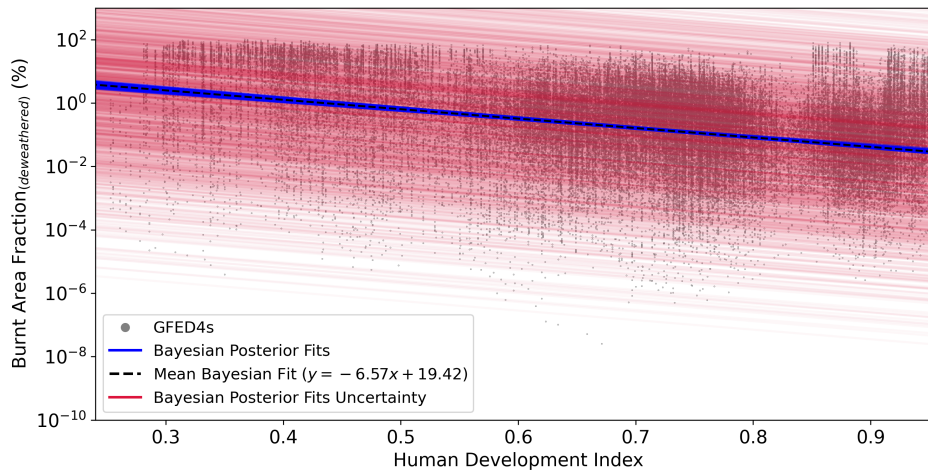
**Figure 2.** Pearson correlation (%) coefficient between the monthly mean (1997 – 2016) a) FWI and the deweathered Burnt Area (GFED4s), and b) HDI and the deweathered Burnt Area (GFED4s). Stippling is shown for indicates grid points where the Pearson correlation is statistically significant with a 95% confidence level after controlling for the false discovery rate using the Benjamini and Yekutieli (2001) procedure.

Figure 2 – there is and HDI is not statistically significant. In the regions where the correlation is significant, there is generally a stronger negative correlation between HDI and the deweathered burnt area for most of the globe, relative to what is found for FWI, except for compared to FWI, with notable exceptions in the Indian subcontinent and Eastern China, which shows where a positive correlation – The relation between HDI and the deweathered burnt area is especially is observed. The negative relationship is particularly evident over Eurasia, continental North America, central Asia, Southern Africa, and Australia. For these regions, despite the Eastern and Western Australia, where increases in FWI, burnt area has shown a variety of negative regional trends highly coexist with regional decreases in burnt area that are significantly correlated with HDI (Figure Figures 1 and 2). Nonetheless, the deweathered burnt area shows a strong positive correlation with FWI over the boreal regions of North America and Siberia, as well as the Cerrado ecoregion of South America.

Multiple techniques are used to further investigate the relationship between HDI and burnt area. The scatter plot of the deweathered burnt area against HDI in log-transformed natural space is presented in Figure 3. Due to the inherent stochasticity of burnt area, the results show a wide range of values, spanning small to large relative burnt area fractions for any given HDI. To account for this variability, and isolate the effects of HDI on burnt area, we applied a Bayesian Linear Regression method (Klauenberg et al., 2015) to the log-transformed burnt area fraction, denoted by  $\log(BA^*)$ :

$$\log(\log(BA^*)) \sim BA_0 + \delta BA \times HDI \quad (4)$$

where  $BA_0$  is the burnt area intersect represents the expected log-burnt area at  $HDI = 0$ , and  $\delta BA$  is the change, or slope, represents the change in burnt area with HDI. We optimise using a No U-Turn log-burnt area with HDI. We assumed that  $\log(BA^*)$  is normally distributed centred on the linear predictor, with residual standard deviation  $\sigma$  treated as an additional parameter with a half-normal prior. Priors for the regression coefficients were chosen to be weakly informative:



**Figure 3.** Relation between the ~~between the~~ monthly mean (1997–2016) HDI and the ~~log transform~~ burnt area fraction (%) for GFED4s. The grey dots represent the ~~GFED4s scatter plot for all monthly~~ burnt area ~~fraction in values at all grid cells as a function of HDI, the~~. The Bayesian regression posterior fits ~~is are~~ represented ~~in by~~ blue solid lines, the mean Bayesian fit is represented ~~in by~~ the black dashed line, and the uncertainty from the Bayesian posterior ~~fits fit~~ residuals is represented ~~in the by~~ red solid lines. ~~Although the Bayesian regression was performed in log-transformed space, the results are presented here in natural space for interpretability.~~

~~$BA_0 \sim \mathcal{N}(0, 25)$  and  $\delta BA \sim \text{LogNormal}(0, 10)$ , reflecting uncertainty in both the intercept and the HDI effect while constraining  $\delta BA$  to positive values.~~

270 ~~The model was fitted using monthly burnt area and HDI data from all grid cells, allowing short-term variability to be smoothed and the longer-term relationship between HDI and burnt area to be quantified. Posterior inference was carried out using the No-U-Turn Sampler (NUTS) optimisation over a normal posterior distribution, using implemented in the PyMC Python package, as per Kelley et al. (2019).~~

275 ~~The priors for our two regression parameters were largely uniformed, with  $BA_0$  having a normal distribution, with a mean of zero and a standard deviation of 25, and  $\delta BA$  having a log-normal distribution with mean of zero and standard deviation of ten (Kelley et al., 2019). Convergence was verified via R-hat values  $< 1.01$ , and 1000 posterior draws were generated to quantify parameter uncertainty. Although the Bayesian regression was performed in log-transformed space, the results are presented here in natural space for interpretability.~~

280 ~~We utilise 1000 Bayesian posterior model fits (with To visually represent the uncertainty, 145 samples represented by the solid blue line posterior draws were plotted as solid blue lines in Figure 3), effectively capturing the uncertainty in the data while estimating the association. This number was chosen pragmatically to provide a sufficiently large sample size to capture posterior variability while avoiding excessive clutter in the figure, ensuring a clear representation of both the spread and central tendency of the predicted relationship between HDI and burnt area.~~

285 This method ~~show shows~~ that the observations show a linear decline in burnt area with increasing HDI, with a ~~posterior~~ mean slope of -6.57 (%).

### 2.3 INFERNO fire model

In this work we simulate fire using the INFERNO (INteractive Fires and Emissions algoRithm for Natural enviroNments; Mangeon et al. (2016)) fire model. INFERNO uses an approach based on Pechony and Shindell (2009), adapted to allow interactions within an ESM framework. More precisely, INFERNO uses water vapour pressure deficit as one of the main indicators of flammability and an inverse exponential relationship to relate flammability to soil moisture.

$$BA_{PFT} = I_T F_{PFT} \overline{BA_{PFT}} \quad (5)$$

where  $I_T$  represents the fire ignitions, including natural and human ignitions as well as fire suppression by humans,  $F_{PFT}$  the flammability per PFT dependent on the 1.5 m temperature, 1.5 m relative humidity and fuel density - as defined in Eq. 4 through 6 from Mangeon et al. (2016) - and  $\overline{BA_{PFT}}$  is the average burnt area for each PFT.

The burnt area, represented in Eq. 5, is associated with the average burnt area per fire for each model plant functional type (PFT). This decouples the fire spread stage from local meteorology and topography, processes not typically resolved in coarse grids, such as those often used within ESMs. fire spread from localised effects of wind, weather, or topography, which are not resolved at the coarse spatial scales used in ESMs. Instead, INFERNO relies on PFT-specific flammability and fire occurrence metrics, capturing broad-scale, climate and vegetation-driven fire dynamics. This approach does not explicitly represent sub-grid heterogeneity in topography or local meteorology, which is a limitation that may influence local fire spread.

It should be noted that the recent work by Haas et al. (2022) shows that topography and wind speed have an impact on fire size even when aggregated to a  $0.50^\circ$  grid cell scale. However, the resolution of the model used in this study is significantly coarser - approximately  $1.75^\circ$ .

INFERNO fire ignitions are split into Natural Ignitions ( $I_N$ ) from cloud to ground lightning flashes and from Human activities ( $I_A$ ) dependent on population density ( $PD$ ) as described in Eq. 6. Humans are also responsible for suppressing fires in the model, using a suppression function ( $f_{NS}$ ) dependent on human population density (Eq. 7) to represent the fraction of fires not suppressed by humans. The total ignitions ( $I_T$ ) are represented by Eq. 8.

$$I_A = k_{(PD)} PD \alpha \times (\mathbf{1} - \mathbf{HDI}) \quad (6)$$

$$f_{NS} = 7.7 (c_1 + c_2 \times e^{-\omega PD}) \times (\mathbf{1} - \mathbf{HDI}) \quad (7)$$

$$I_T = (I_N + I_A) \frac{f_{NS}}{8.64 \times 10^{10}} \quad (8)$$

where  $k_{(PD)} = 6.8 \times PD - 0.6$  is a function that represents the varying anthropogenic influence on ignitions in rural versus urban environments, and the parameter  $\alpha = 0.03$  represents the number of potential ignition sources per person per month per  $km^2$ , and  $HDI$  represents the Human Development Index.

315 In Equation 7 the fraction of fires that remain unsuppressed at the most populated areas is expressed by  $c_1$ . The maximum number of fires that remain unsuppressed at the distant, unpopulated regions is defined by the sum of  $c_1$  and  $c_2$ , and the rate at which the number of unsuppressed fires decreases with increasing population density is determined by  $\omega$ . As expressed by Pechony and Shindell (2009), due to the lack of global quantitative data, constant values are selected in a rather heuristic manner:  $c_1 = 0.05$ ,  $c_2 = 0.9$ , and  $\omega = 0.05$ . In this way, up to 95 % of fires are assumed to be suppressed in densely populated  
320 regions, and 95 % are assumed to remain unsuppressed in unpopulated regions.

Previously, INFERNO only included information on population density. To represent the socio-economic factors impacting fire ignition and suppression, we include a HDI term ( $1 - HDI$ ) in our human ignition and suppression Eq. 6 and 7 (shown in bold). In addition it should be noted that the HDI implementation scales both  $c_1$  and  $c_2$  according to the HDI value of any given grid point.

325 This approach does not directly implement the empirical relationship established from observational data in Section 2.2. Instead, it introduces an HDI dependent formulation based on the assumption that ignition rates decrease and suppression increases with higher HDI. This reflects the hypothesis that more developed regions experience fewer ignitions and greater fire control capacity. We then test whether this indirect implementation can reproduce the observed relationship between burned area and HDI.

330 Despite being a simple representation, it aligns with the few studies found in literature that looked at the impact governmental policies have on prevention of wildfires (e.g., the work by Curt and Frejaville (2018)). Furthermore, although the equations used could be adjusted to provide the best results, we avoid this approach in this first implementation in INFERNO to avoid masking compensating biases that are existent or could arise from this implementation.

In this representation of socio-economic impacts on fire ignition and suppression, we assume that fire ignitions decrease and  
335 fire suppression increases for areas with more effort in human development improvements. Moreover, it reduces the impact changes in population density have in areas with high HDI while keeping a dependency on population density changes for areas with low HDI, where policies on land and fire management have a greater role than other human behaviours in controlling ignitions (Nikolakis and Roberts, 2022; Ford et al., 2021; Jacobson et al., 2022; Carreiras et al., 2014; Mourão and Martinho, 2014). The impact of HDI on INFERNO anthropogenic fire ignitions and suppression, represented as  $I_A$  (Eq. 6) and  $f_{NS}$  (Eq. 7) respectively, is depicted in Figure 4.

We obtained HDI data from the gridded global datasets for Gross Domestic Product and Human Development Index (Kummu et al., 2018), which provides HDI data from 1990 to 2015. To cover the full modelled period (1860-2016), the HDI data is linearly ramped from the minimum HDI value of the dataset (0.2) to its value in 1990 for each grid point. The original HDI dataset was spatially interpolated using a nearest-neighbor interpolation method to match the model grid, and was updated at  
345 the same frequency as the original ~~dataset~~ dataset - annually.

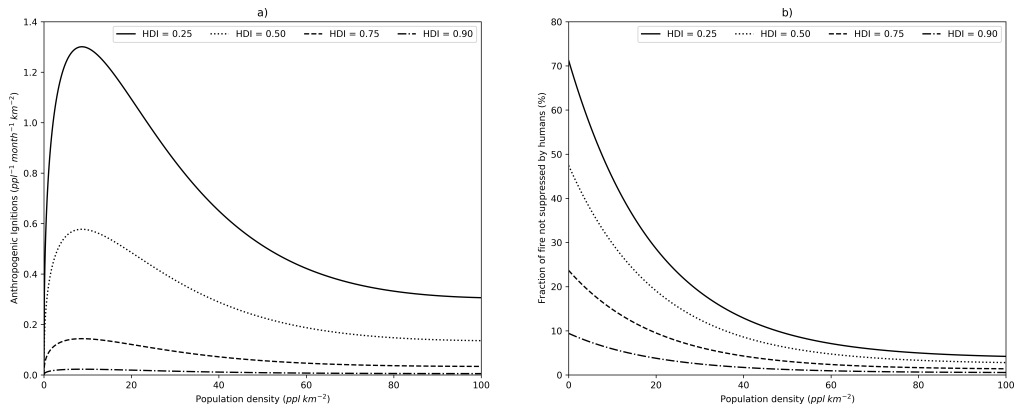


**Figure 4.** Anthropogenic fire ignitions ( $ppl^{-1} month^{-1} km^{-2}$ ) a) and fraction of fire not suppressed by humans (%) b) as a function of population density ( $ppl km^{-2}$ ) and Human Development Index.

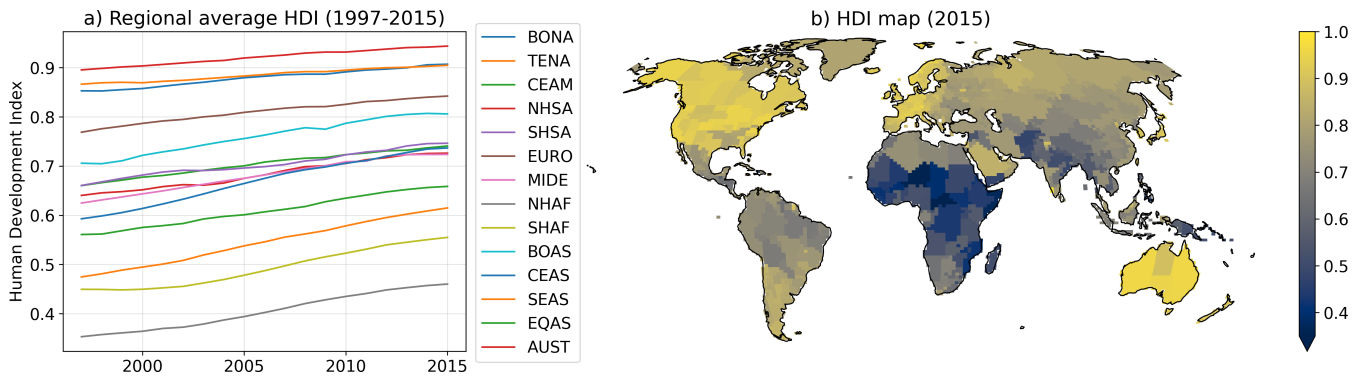


**Figure 5.** RegridDED HDI as provided to JULES-INFEERNO+HDI. a) regional average for the 1997-2015 period and b) spatial distribution for the year 2015. The regions depicted in a) are described in Figure A1.

## 2.4 JULES-ES and INFERNO

We use the community land surface model JULES (Joint UK Land Environment Simulator; Clark et al. (2011); Best et al. (2011)) at version 5.7, with the science configuration of the land surface as used in UKESM1 (Sellar et al., 2019a), including 13 PFTs, and dynamic vegetation from TRIFFID (Top-down Representation of Interactive Foliage and Flora Including Dynamics; 350 Cox et al. (2000); Cox (2001)). This ES configuration of JULES is known as JULES-ES (Mathison et al., 2022). JULES simulates surface fluxes of water, energy, as well as vegetation and carbon. Here, we use JULES as a stand-alone offline model run at a spatial resolution of N96 (equivalent to a horizontal resolution of 135 km in the mid-latitudes). The Climate Research Unit - National Centers for Environmental Predictions reanalysis (CRU-NCEP v7) (Harris et al., 2014; Viovy, 2018) atmospheric variables are provided at 6-hourly intervals to drive JULES, including carbon dioxide ( $CO_2$ ), precipitation,

355 temperature, specific humidity, wind, air pressure, and short and long wave radiation. The model runs from 1860–2016 with  
this forcing. In this work, we analyse the period that overlaps with observations (1997–2015).

We use the ~~latest fire-vegetation fire-vegetation~~ coupling described in ~~Burton et al. (2019) and Burton et al. (2020), incorporating~~  
~~additional feedbacks to the carbon cycle~~ Burton et al. (2019, 2020), which incorporates additional carbon cycle feedbacks from  
litter and vegetation burning. ~~This setup includes mortality due to fire and explicitly accounts for fire-induced mortality~~ by  
360 plant functional type (PFT), ~~which is~~. Mortality rates, set to 40 % for trees, 60 % for shrubs, and 100 % for grasses, are based  
on literature values and the methodology documented in Burton et al. (2019), which includes a comprehensive evaluation  
of the model performance in representing the evolution of vegetation within the context of JULES-INFERNO model. This  
setup differs from that used in Teixeira et al. (2021), ~~where no fire-vegetation feedbacks were considered, which did not~~  
~~include fire-vegetation feedbacks~~. While simplified, these PFT-specific mortality parameters are intended to capture large-scale  
365 patterns of fire-driven vegetation change rather than site-specific fire regimes.

This approach represents a simplification of real-world fire processes. Due to spatial resolution and computational constraints,  
global fire modelling frameworks necessarily abstract the diversity and complexity of fire behaviour across ecosystems, and  
variations in fuel type, structure, and landscape heterogeneity are not fully resolved at the model scale. Despite these limitations,  
coupling with JULES allows INFERNO to capture broad spatial and temporal patterns in fuel availability consistent with  
370 large-scale vegetation dynamics and meteorological conditions.

Fire ignitions are based on population density data from HYDE 3.2 (Klein Goldewijk et al., 2017); (Goldewijk et al.,  
2017) and monthly lightning ~~flashes climatology from LIS-OTD~~ flash climatology from LIS-OTD (Lightning Imaging ~~Sensor~~  
~~—Optical-Sensor-Optical~~ Transient Detector; Cecil (2006)) observations over ~~1995-2014~~ 1995–2014, regrided from  $0.5^\circ$   
resolution to N96 ( $1.25^\circ$  ~~+25 latitude × latitude ×~~ 1.875° longitude). The LIS-OTD climatology provides total lightning  
375 flash density (including both intra-cloud and cloud-to-ground flashes); following Christian et al. (2003), total lightning flashes  
are converted to cloud-to-ground flash density using an empirical partitioning based on observed global relationships between  
total and cloud-to-ground lightning. After spinning up the model to equilibrium, we complete a full historical simulation from  
~~1860-2019~~ 1860–2019 at N96 and use results from the present day period (1997–2015) for our analysis ~~to compare with,~~ which  
are compared against available observations of ~~burnt~~ burned area.

380 We performed two model experiments to test the impact of representing the socio-economic factors on fire ignition and  
suppression in INFERNO. A control experiment referred to as JULES-INFERNO, and a similar experiment, including representing  
the socio-economic factors through HDI on fire ignition and suppression parametrisation described in section 2.3, referred as  
to JULES-INFERNO+HDI.

Socio-economic impacts on fire are not represented in the initial formulation of INFERNO described in Mangeon et al.  
385 (2016) for the ignitions and suppression of fires. ~~This is reflected in,~~ which affects the  $\overline{BA_{PFT}}$  values used in the initial  
implementation of INFERNO. Posterior work by Andela et al. (2019) shows that average burnt area values can be larger than  
the ones used in the work of Mangeon et al. (2016).

When the HDI-based parametrisation of socio-economic impacts on fire is included in INFERNO, it reduces ignitions and  
suppression of fires. Therefore, the values of  $\overline{BA_{PFT}}$  are adapted to align with those reported by Andela et al. (2019). This

**Table 1.** Biomass burning average burnt areas ( $km^2 fire^{-1}$ ) for ~~various~~ all JULES plant functional types ~~based~~ used in this configuration. Based on Burton et al. (2019) (top row) and adapted from Andela et al. (2019) (bottom row).

	Broadleaf tree			Needleleaf tree		C3			C4			Shrubs	
	Deciduous	Evergreen		Evergreen	Deciduous	Grass	Crop	Pasture	Grass	Crop	Pasture	Deciduous	Evergreen
		Tropical	Temperate										
$\overline{BA_{PFT}}$	1.7	1.7	1.7	1.7	1.7	3.2	0.4	3.2	3.2	0.4	3.2	2.7	2.7
Revised $\overline{BA_{PFT}}$	5.2	1.4	2.5	5.2	5.2	10.2	1.4	1.4	10.2	1.4	1.4	5.1	5.1

390 was achieved by deriving the PFT-specific values by matching those reported by Andela et al. (2019) to the PFT categories represented in JULES as much as possible. These are not direct comparisons and a balance between the PFT representation of the region in JULES was used to estimate a reasonable average burnt area for INFERNO. The  $\overline{BA_{PFT}}$  values in both experiments are detailed in Table 1.

## 2.5 Burnt area evaluation

395 ~~To analyse the model performance, we calculated the following statistical and error measures, relative to the observed (GFED4s) and modelled (JULES-INFERNO and JULES-INFERNO+HDI) burnt area :-~~

- ~~– Deviation of the modelled data in relation to observed values:-~~

$$\phi'_i = \phi_i - \phi_{i,obs}$$

- ~~– Bias, which represents the mean deviation of the modelled data in relation to the observed values.-~~

400 
$$Bias = \frac{1}{N} \sum_{i=1}^N \phi'_i$$

- ~~– The Root Mean Square Error.-~~

$$RMSE = \sqrt{\frac{\sum_{i=1}^N (\phi_i - \phi_{i,obs})^2}{N}}$$

- ~~– The Root Mean Square Error after the removal of a constant bias.-~~

$$RMSE_{UB} = \sqrt{\frac{\sum_{i=1}^n [(\phi_i - \bar{\phi}) - (\phi_{i,obs} - \bar{\phi}_{obs})]^2}{N}}$$

- 405 ~~– Standard deviation for the modelled – equation A5 – and observed – equation A6 – data.-~~

$$STD = \sqrt{\frac{\sum_{i=1}^n (\phi_i - \bar{\phi})^2}{N}}$$

$$STD_{obs} = \sqrt{\frac{\sum_{i=1}^n (\phi_{i,obs} - \bar{\phi}_{obs})^2}{N}}$$

where  $i$  is the temporal index and  $N$  is the number of elements of  $\phi$  considered, and  $\bar{\phi}$  is the constant bias.

Considering these statistics, a perfect simulation would have the following criteria:-

- 410
- ~~RMSE = 0~~
  - ~~RMSE<sub>UB</sub> = 0~~
  - ~~bias = 0~~
  - ~~Pearson correlation = 100 %~~
  - ~~STD / STD<sub>GFED4s</sub> = 1~~

415

    - ~~RMSE / STD<sub>GFED4s</sub> = 0~~
    - ~~RMSE<sub>UB</sub> / STD<sub>GFED4s</sub> = 0~~

Although INFERNO has been used in other studies to estimate fire-related emissions, this manuscript focuses exclusively on assessing the influence of the Human Development Index (HDI) on fire activity and on evaluating model performance in simulating burned area fractions. Fire emissions are therefore not analysed in this study.

## 420 3 Results

### 3.1 Representing Burnt Area - HDI relationship in INFERNO

The posterior fit distributions of the Bayesian Linear Regression parameters slope, intercept and sigma (~~additional noise residual variability~~ caused by none HDI drivers) in Figure 3 and 7 show narrow intervals for the posterior parameters, evidence of high confidence in the fit for a linear relationship between HDI and deweathered burnt area fraction, with the mean Bayesian  
425 fit (dashed black line) presenting a slope of  $-6.57 (\%^{-1})$ , and an intercept of 19.42 (%).

In summary, this analysis reveals a strong relationship between the HDI and burnt area (Figure 7). It demonstrates a predominantly negative correlation between HDI and deweathered burnt area globally, and especially in Eurasia, continental North America, central Asia, Southern Africa, and Australia, where increases in FWI have not translated into higher burnt areas (Figure 2). Conversely, positive correlations persist in regions like the boreal areas of North America, Siberia, and the Cerrado  
430 of South America. This evidence highlights suggests that HDI can ~~be used as an indicator of the role regionally capture part of the variability in burned area, reflecting some influence of~~ socio-economic factors ~~play in mitigating fire activity.~~

To evaluate the use of HDI as a proxy for representing socio-economic factors influencing fire ignition and suppression in INFERNO, the methodology described in Section 2.2 was applied, and the results are presented in Figure 6, and the distribution of its posterior fits can be found in Figure 7.

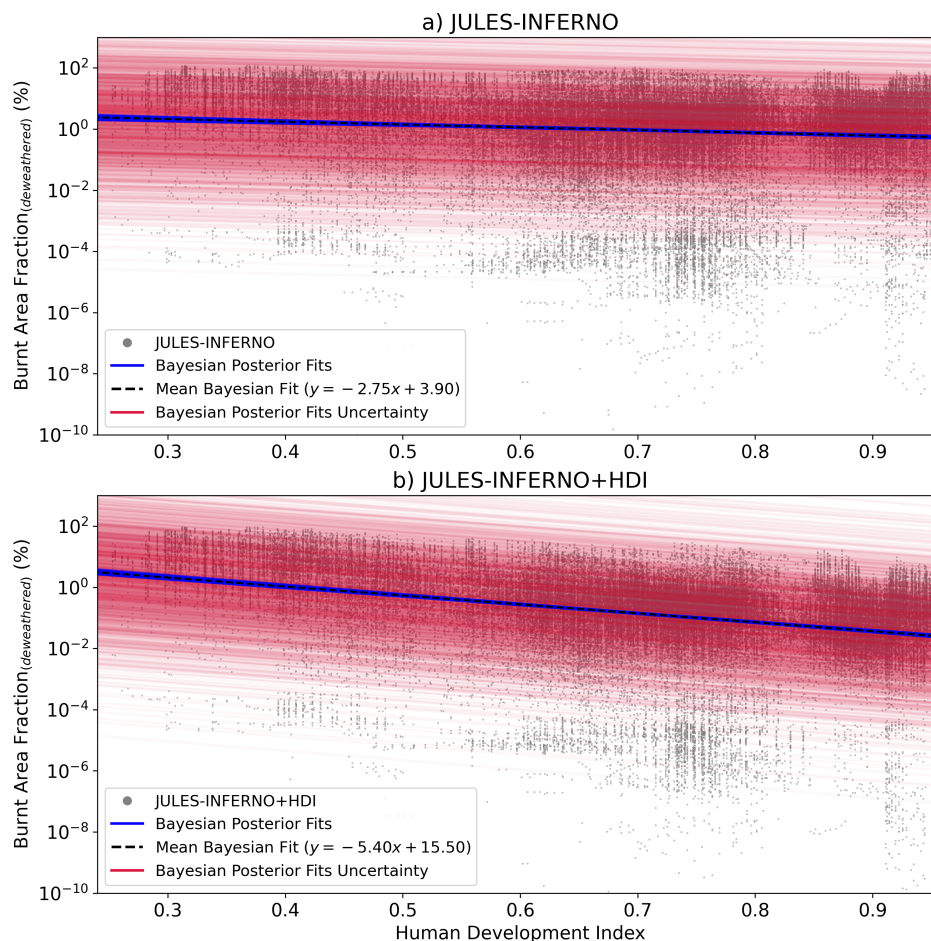


**Figure 6.** Relationship between the monthly mean (1997–2016) HDI and the ~~log-transformed~~ burnt area fraction (%) for (a) JULES-INFERNO and (b) JULES-INFERNO+HDI. The grey dots represent the scatter plot for all monthly burnt area fraction values at all grid cells as a function of HDI. The blue solid lines indicate the Bayesian regression posterior fits, while the black dashed line shows the mean Bayesian fit. The red solid lines depict the uncertainty from the Bayesian posterior fit residuals. Although the Bayesian regression was performed in log-transformed space, the results are presented here in natural space for interpretability.

435 As expected, JULES-INFERNO (the original version of the model not including the HDI) does not present a strong relationship between the deweathered burnt area fraction and HDI. The mean Bayesian fit slope is  $-2.75$  (%), indicating a weaker relationship between the variables than in JULES-INFERNO+HDI when compared to observations. In contrast, the stronger negative slope of  $-6.57$  ( $\%^{-1}$ ) found in observations suggests a more pronounced socio-economic influence on fire

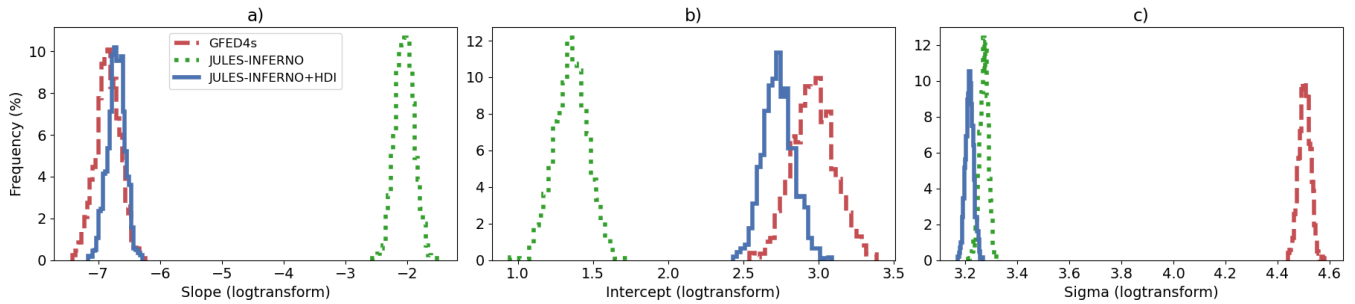


**Figure 7.** Histograms of posterior distributions for Bayesian linear regression fit parameters derived for GFED4s (dashed red line), JULES-INFERNO (dotted green line), and JULES-INFERNO+HDI (solid blue line). Panel a) shows the slope parameter, b) the intercept parameter, and c) depicts the sigma (error term representing random sampling noise) in log-transformed space.

suppression in the observational data. When HDI is explicitly incorporated to represent socio-economic effects on fire in  
 440 JULES-INFERNO+HDI, the model better reproduces the relationship observed in GFED4s, with a Bayesian fit slope of  $-5.40$  ( $\%^{-1}$ ). This result demonstrates an improved representation of the socio-economic impact on fire dynamics, aligning the model more closely with observations in terms of global mean dependence on HDI.

### 3.2 Evaluation of impact on burnt area

To better understand the regional impact of implementing the socio-economic factors on fire ignition and suppression in  
 445 INFERNO, we focus on the burnt area results averaged over the GFED4s regions as defined in Figure A1.

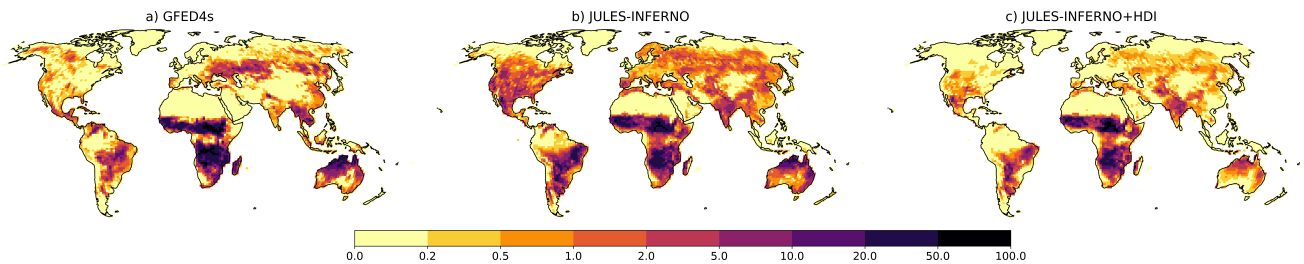


**Figure 8.** Burnt area fraction (%) mean annual average (1997 - 2016) for a) GFED4s, b) JULES-INFERNO and c) JULES-INFERNO+HDI. Please note that the colour mapping uses a colour axis in which the difference in colours do not correspond linearly to differences in burnt area fraction.

Both model experiments reproduce the overall geographical pattern of the annual average burnt area fraction (Figure 8), though with some regional differences compared to observations. For instance, JULES-INFERNO simulates the observed pattern in the major fire regions: South America, Africa and Eurasia. The 2-D cross-correlation was used to determine what is referred to as spatial correlation between the model experiments and the observation data. JULES-INFERNO shows substantial  
 450 spatial biases over North America, Europe and Asia, leading to a low global spatial correlation of ~~26.5%~~ 0.265 compared with

GFED4s. Conversely, JULES-INFERNO+HDI reduces fires in the regions with higher HDI values, reducing the biases seen in JULES-INFERNO and resulting in a better agreement with GFED4s. JULES-INFERNO+HDI has a global spatial correlation of ~~46.5%~~ 0.465 when compared with GFED4s. However, due to the nature of the HDI data, sharp boundaries between countries can appear in the burnt area results (e.g., between Canada and the United States of America) - 1 e).

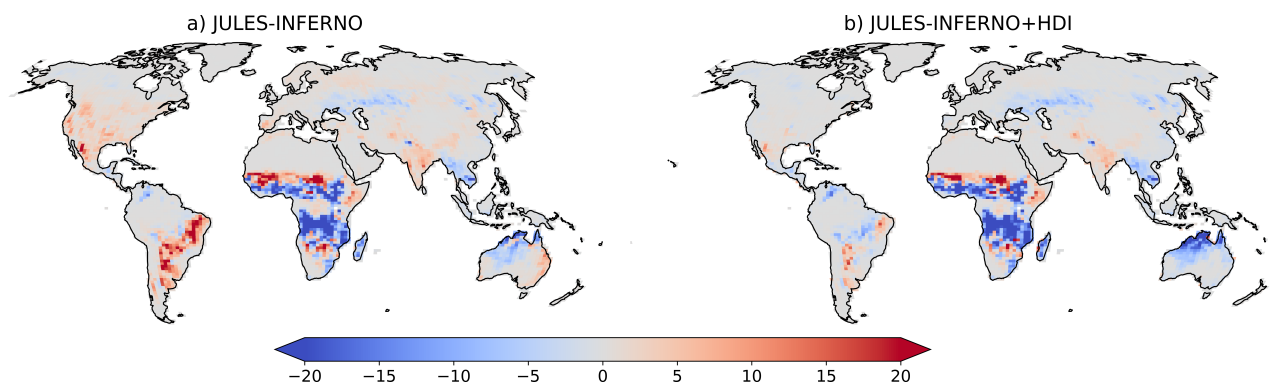


**Figure 9.** Burnt area fraction (%) mean annual average bias (1997 - 2016) for a) JULES-INFERNO, and b) JULES-INFERNO+HDI, calculated relative to the GFED4s observations

455 ~~Including~~ Representing the socio-economic factors through HDI in the parametrisation for fire ignition and suppression has an impact in all regions. However, it mostly reduces the burnt area in regions with high prosperity (high values of HDI), leading to ~~improvements~~ reduced bias over North America, Europe and Asia, as shown in Figure 9. Moreover, compared to JULES-INFERNO, JULES-INFERNO+HDI reduces the positive bias over South America and India, although it increases the negative bias over the boreal regions, Australia, and South East Asia.

460 To further evaluate the impact of incorporating socio-economic factors on fire dynamics in INFERNO via HDI, we present histograms depicting the frequency distribution of burnt area across different fire regions in Figure 10. These histograms provide valuable insights into how the inclusion of socio-economic factors in JULES-INFERNO+HDI influences the occurrence of fires of different magnitudes compared to both JULES-INFERNO and GFED4s observations. To provide a quantitative assessment of model performance, the Wasserstein distance (Ramdas et al., 2017) is used as a metric of the fit between the probability distributions of the JULES-INFERNO and JULES-INFERNO+HDI histograms and the GFED4s observations.

465 In this context, smaller values indicate better agreement between modelled and observed distributions, with a value of zero representing a perfect match and progressively larger values reflecting increasing divergence. This analysis helps to identify the dominant fire sizes in each region, assess whether the introduction of socio-economic factors leads to shifts in these distributions, and determine if whether the implementation in JULES-INFERNO+HDI leads to a better ~~representations~~ representation

470 of the burnt area probability distribution.

Globally, GFED4s observations display a steep decline in burnt area frequency as fire sizes increase, with small burnt area fractions dominating the distribution ~~-Both Both~~ (Figure 10a). JULES-INFERNO ~~and JULES-INFERNO+HDI exhibits~~ an-reproduces this dominance of small fires relatively well but exhibits a strong underestimation of the frequency of larger

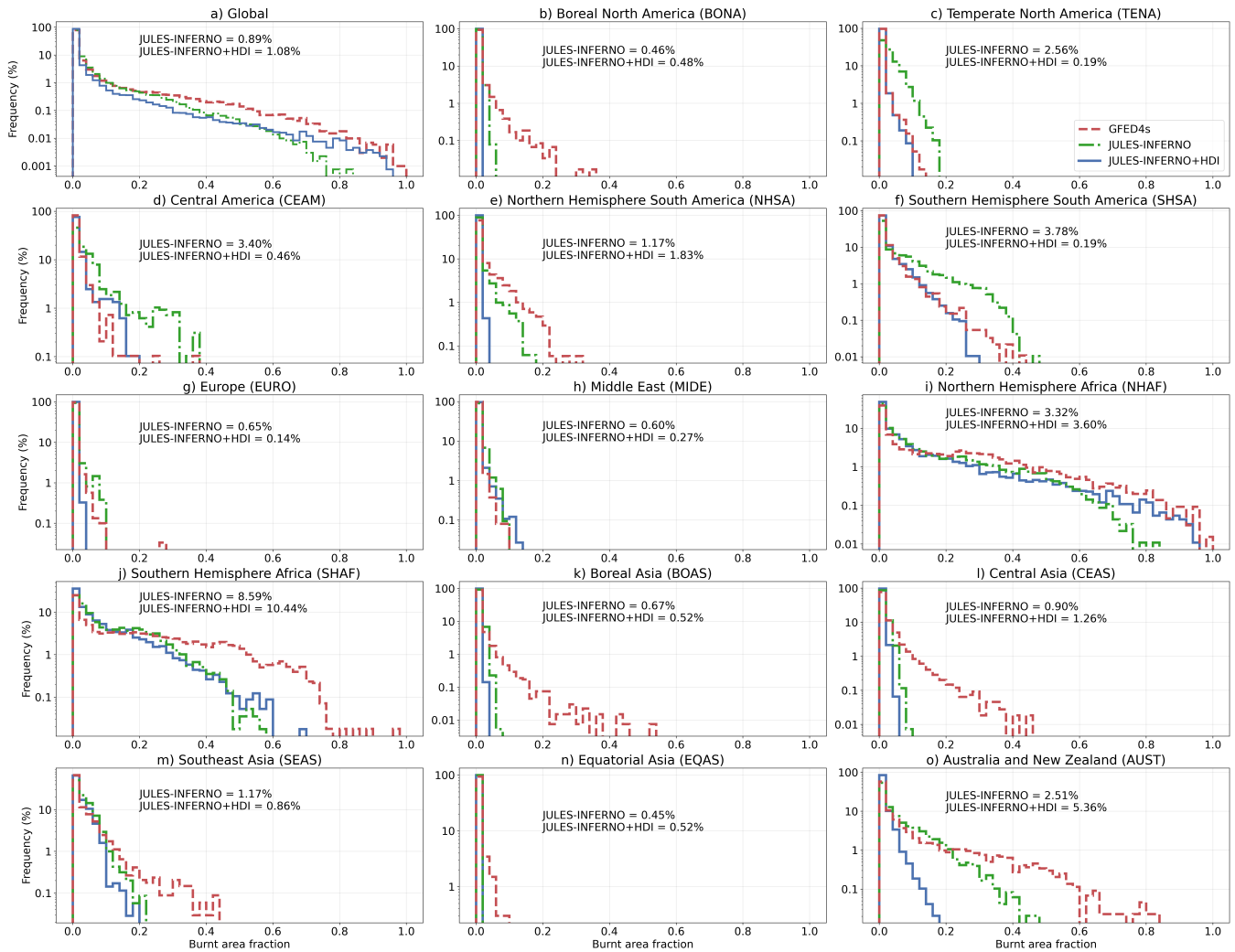


**Figure 10.** Histograms showing the distribution of burnt area fractions across fire regions for GFED4s observations (red dashed lines), JULES-INFERNO (green dotted lines), and JULES-INFERNO+HDI (blue solid lines), for the different fire regions. Annotated values indicate the Wasserstein distance of each model experiment relative to GFED4s.

burnt areas in the range of 0.3 to 0.7. By incorporating HDI to represent these factors together with revised parameters for  $\overline{BA_{PFT}}$ , large burnt area fractions ( $> 0.5$ ). The introduction of HDI in JULES-INFERNO+HDI increases the frequency of large burnt areas, resulting in a distribution that more closely aligns with GFED4s, particularly for fire sizes between HDI increases the frequency of the largest burnt area fractions (0.7 and 1.0), improving the representation of larger fire sizes relative to JULES-INFERNO. However, this improvement comes at the expense of degraded performance for small to moderate burnt area fractions ( $< 0.5$ ), which account for the majority of fire occurrences. This trade-off is reflected in the Wasserstein distance, which increases slightly from 0.89 % for JULES-INFERNO to 1.08 % for JULES-INFERNO+HDI at the global scale, indicating that despite the improved fit for extreme fires, this does not compensate for the deterioration across more frequent smaller fires.

In boreal regions (Boreal North America (BONA), BONA, and Boreal Asia (BOAS)), GFED4s observations show distributions dominated by smaller distributions are strongly skewed towards small burnt areas, with a rapid decline in frequency as fire size increases. In contrast, both beyond 0.1. Both JULES-INFERNO and JULES-INFERNO+HDI substantially under-represent moderate to large burnt areas, particularly above size fires in these regions (burnt area fractions between 0.1 and 0.4), indicating persistent challenges in capturing boreal fire dynamics. The inclusion of HDI leads to a modest additional suppression of burnt areas, but the resulting Wasserstein distances remain very similar between the two model configurations (0.46 % for JULES-INFERNO and 0.48 % for JULES-INFERNO+HDI in BONA and 0.67 % for JULES-INFERNO and 0.52 % for JULES-INFERNO+HDI in BOAS). This indicates that incorporating socio-economic factors does not provide a clear improvement or degradation in the overall agreement with observations in boreal regions, suggesting that other processes, such as fuel availability, fire weather, or ignition sources, are likely more influential in governing boreal fire regimes.

Temperate regions, such as Temperate North America (TENA) and Europe (EURO), exhibit fire dynamics characterized by a GFED4s observations again show a strong dominance of small burnt areas, with GFED4s showing a steep decline in fire frequency as fire size increases. fires (burnt area fractions  $< 0.1$ ). In TENA, JULES-INFERNO over-predicts the frequency of larger burnt areas in both regions, particularly above markedly overestimates burnt area fractions greater than 0.1, highlighting the model's limitations in representing fire suppression. The introduction of HDI in while JULES-INFERNO+HDI results in a marked reduction in the overestimation of large fires in TENA, improving the agreement with observations. In EURO, the inclusion of socio-economic factors better represents both substantially reduces this bias. This improvement is quantitatively supported by a pronounced reduction in Wasserstein distance from 2.56 % to 0.19 %, indicating a clear overall improvement across the full distribution. For EURO, although JULES-INFERNO+HDI reduces the occurrence of larger fires, it also underestimates small and moderate burnt area fractions, suggesting a more accurate reflection of the extensive fire suppression practices typical of developed regions. Consequently, the Wasserstein distance decreases from 0.65 % in JULES-INFERNO to 0.14 % in JULES-INFERNO+HDI, suggesting a closer overall distributional match, but Figure 10g shows that this improvement does not consistently reflect better performance across all fire size classes. In particular,

JULES-INFERNO better captures the frequency of small fires, which dominate the observed distribution, indicating that the apparent improvement in the Wasserstein distance should be interpreted cautiously.

510 In ~~regions such as~~ Central America (CEAM) and Southern Hemisphere South America (SHSA), GFED4s ~~shows broader frequency distributions, with a more gradual decline in frequencies and significant~~ exhibits broader distributions with contributions from small ~~and to~~ moderate burnt areas. JULES-INFERNO strongly ~~over-predicts burnt areas frequencies, particularly above 0.1, indicating an inadequate representation of fire suppression dynamics. JULES-INFERNO+HDI narrows this distribution, reducing the overestimates moderate and large fires in both regions, leading to large Wasserstein distances (3.40 % and 3.78 %,  
515 respectively). The inclusion of HDI substantially narrows the distributions and reduces the occurrence of large fires and better capturing the observed frequencies.~~

, resulting in marked reductions in Wasserstein distance (to 0.46 % in CEAM and 0.19 % in SHSA). These results indicate a genuine improvement across most of the distribution, including the dominant fire sizes. In African savanna regions (Northern Hemisphere Africa(NHAF), NHAF, and Southern Hemisphere Africa(SHAF)are regions where the frequency of larger burnt  
520 areais higher than in other regions according to GFED4s. Both model configurations underestimate large burnt areas, though, SHAF), GFED4s shows relatively high frequencies of large burnt areas. Both experiments underestimate extreme fire sizes, but JULES-INFERNO+HDI shows an improved representation by increasing the frequency of extreme fire sizes, particularly in NHAFincreases the suppression of medium fires further, leading to mixed results. In NHAF, the Wasserstein distance increases from 3.32 % in JULES-INFERNO to 3.60 % in JULES-INFERNO+HDI, while in SHAF it increases from 8.59 % to 10.44 %,  
525 indicating a degradation in overall distributional agreement despite improvements in larger fire sizes.

For the Asian regions, such as Equatorial Asia (EQAS), Central Asia (CEAS), East Asia (SEAS) Across Asian regions (EQAS, CEAS, SEAS) and Australia and New Zealand (AUST), GFED4s demonstrates a dominance of medium to small burnt areas. Both model configurations tend to distributions are dominated by small to moderate burnt area fractions. Both experiments under-predict medium fire sizes medium-sized burnt area fractions (e.g., between 0.2 and 0.6) when compared to  
530 observations, with JULES-INFERNO+HDI showing further increase of generally exacerbates this negative bias, particularly in AUST. This is reflected in increased Wasserstein distances for JULES-INFERNO+HDI in CEAS (1.26 % for JULES-INFERNO and 0.90 % for JULES-INFERNO+HDI) and AUST (2.51 % for JULES-INFERNO and 5.36 % for JULES-INFERNO+HDI), indicating that the additional suppression associated with HDI reduces agreement with observations across the most frequent fire sizes.

535 By introducing Overall, the introduction of a socio-economic representation of fire suppression, in JULES-INFERNO+HDI reduces the frequency of large burnt areas in many regions, addressing overestimations in burnt area that were prevalent in the original and corrects strong positive biases present in JULES-INFERNO configuration. This improvement is particularly evident in regions such as in several regions, notably TENA, CEAM, SHSA, and NHAF, where socio-economic factors are likely to play a critical role in fire management.

540 Nevertheless, discrepancies remain in some regions, such as NHSA, and AUST, where the model continues to under-predict medium and large fire sizes. These persistent biases suggest that while the inclusion of HDI represents a significant advancement, further refinements in and SHSA. However, these improvements are often accompanied by a deterioration in the representation

of small and moderate burnt area fractions, which dominate fire occurrence globally. As reflected by the Wasserstein distance, JULES-INFERN0+HDI does not consistently outperform JULES-INFERN0 across all regions, particularly in savanna-dominated regions such as Africa, Australia, and parts of Eurasia. These results highlight the need for further refinement of the socio-economic parametrization and consideration of other regional factors may be necessary to achieve more accurate parametrisation and the inclusion of additional region-specific processes to improve the simulation of fire size distributions regionally and globally across all fire regimes.

JULES-INFERN0+HDI has a smaller bias than JULES-INFERN0 at a regional scale, especially in regions where JULES-INFERN0 presented large positive biases. However, the savanna regions in Africa, Australia, and central Eurasia are impacted negatively with negative biases increasing in JULES-INFERN0+HDI.

Figure 11 shows the burnt area annual mean time series. To assess the ability of the model simulations to reproduce the timeseries in comparison with observations observed time series, we perform a statistical analysis based on monthly averaged data, including the calculation of various metrics such as the Root Mean Squared Error (RMSE), Root Mean Squared Error after removal of a constant mean bias (RMSE<sub>UB</sub>), the bias, Pearson correlation, and the Standard Deviation (STD) of the burnt area monthly and annual mean time series for all GFED4s regions (Table A1). The STD is computed after removal of a linear trend. We also assess the model's ability to reproduce observed trends using a simple log-transformed linear regression. Figure 12 summarises these these statistical measures for both model configurations.

The results presented both in Figures 11 and 12, together with the regional statistics in Table A1, show that the inclusion of the socio-economic factors in INFERN0 leads to regional improvements in the simulation of annual burnt area for regions such as Temperate North America (TENA), Central America (CEAM), Southern Hemisphere South America (SHSA), Europe (EURO), consequently reducing the large relative bias found in these regions in the experiments with burnt area in regions where JULES-INFERN0. This bias reduction is especially important for many areas with a substantially large relative bias (bias exhibits the largest deviations from GFED4s (greater than 150 %) in JULES-INFERN0 against observations.

For example, the bias in the TENA region relative bias in TENA is reduced from 735.6 % in JULES-INFERN0 to 44.5 % in JULES-INFERN0+HDI. Other bias reductions include 259.22 % in CEAM from 259.2 % to 24.2 %, in SHSA from 191.7 % to -1.7 %, in EURO from 258.8 % to 24.24 % in CEAM, 191.73 % to -1.72 % in SHSA, 258.81 % to -48.79 % in EURO, and 420.52 % to 231.75 % in MIDE. Conversely, there is -48.8 %, and in MIDE from 420.5 % to 231.8 % (Table A1). These reductions are also accompanied by decreases in RMSE, indicating an improved agreement between JULES-INFERN0+HDI and GFED4s for these regions.

Conversely, some regions experience a smaller, but still noteworthy notable, increase in the relative bias for NHSA from -60.06 % in JULES-INFERN0 to -94.27 % in JULES-INFERN0+HDI, AUST from -21.79 % to -82.29 % relative bias. For example, relative bias in Northern Hemisphere South America (NHSA) changes from -60.1 % to -94.3 %, in Australia (AUST) from -21.8 % to -82.3 %, and SHAF from -45.27 % to -55.31 %, in Southern Hemisphere Africa (SHAF) from -45.3 % to -55.3 %. This highlights that the inclusion of HDI does not uniformly improve model performance in all regions, reflecting a trade-off between correcting large positive biases and potentially amplifying negative biases in other areas.



**Figure 11.** Time series of annual mean burned area (*Mha*) from 1997 to 2016 across different fire regions, shown for GFED4s (solid red line), JULES-INFERNO (green dot-dash line), and JULES-INFERNO+HDI (blue dashed line).

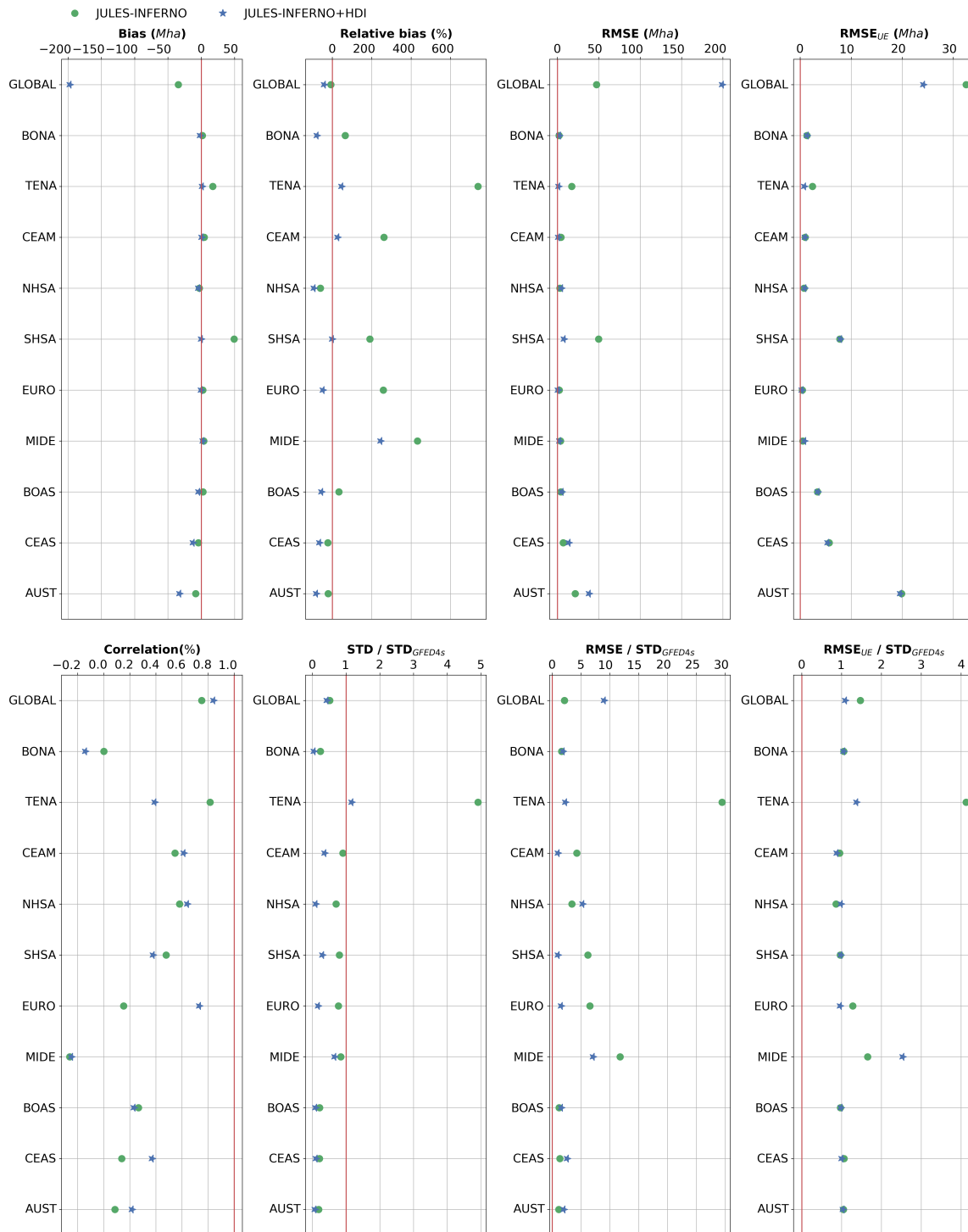


**Figure 12.** Summary of the statistics presented in Table A1 comparing JULES-INFERNO (green circle) and JULES-INFERNO+HDI (blue star). The red line show the reference value for a perfect simulation, the closer the experiment symbol is from this line the better.

Despite the socio-economic factors in INFERNO resulting in a reduction of bias and RMSE in regions where improvements are most needed, it also results in a general ~~In addition, the inclusion of HDI is associated with a systematic~~ reduction in the ~~interannual variability of the burnt area. Although this effect yields improvements in some regions, such as TENA and~~ CEAM, including HDI tends to impact regions which experience high levels of burning negatively. ~~simulated variability.~~ The ratio of modeled to observed standard deviation ( $STD/STD_{GFED4s}$ ), calculated from detrended monthly mean values, decreases in most regions. For instance,  $STD/STD_{GFED4s}$  decreases from 4.41 to 1.04 in TENA, from 0.25 to 0.11 in BONA, from 0.84 to 0.34 in CEAM, from 0.77 to 0.28 in SHSA, and from 0.68 to 0.15 in SHSA, indicating an underestimation of sub-annual variability. While this reduction in variability can contribute to lower RMSE in some regions, it also suggests that in JULES-INFERNO+HDI the amplitude of burnt area fluctuations is damped relative to observations.

These results suggest that, although there is good agreement between the observed mean burnt area and ~~At the global scale,~~ JULES-INFERNO at a global scale (e.g., a bias of  $-7.21\%$ ), this ~~is~~ exhibits a relatively small mean bias due to compensating biases at the regional scale. We find that JULES-INFERNO+HDI performs better overall regionally, improving the representation of global burnt area variability ( $STD / STD_{GFED4s} = 0.99$ ; Table A1), reducing the global RMSE when the constant bias is removed ( $RMSE_{UB}$  is reduced from 32.50 regional errors. The inclusion of HDI reduces these compensating effects, resulting in a larger negative global relative bias (from  $-7.21\%$  in JULES-INFERNO to ~~24.12~~  $-41.46\%$  in JULES-INFERNO+HDI) ~~, and leading to a higher global and an increase in RMSE (from 42.28 to 198.99).~~ Nevertheless,  $RMSE_{UB}$  decreases from 32.50 to 24.12, and the Pearson correlation with GFED4s (~~correlation of 75.25% and 84.19% for increases from 0.75 to 0.84,~~ reflecting an improved representation of temporal co-variability of monthly burnt area.

Overall, the inclusion of socio-economic factors in INFERNO through HDI results in a trade-off. JULES-INFERNO ~~and~~ JULES-INFERNO+HDI respectively; Table A1). Nonetheless, JULES-INFERNO+HDI underestimates the global mean burnt area ~~, resulting in a larger bias when compared to GFED4s~~ improves the mean-state representation in regions with the largest bias in JULES-INFERNO (TENA, CEAM, SHSA, EURO, MIDE). However, relative biases worsen in regions with initial where burnt area is underestimated in JULES-INFERNO (NHSA, SHAF, AUST), and variability is generally reduced.

The ~~Nonetheless, the~~ improvements from JULES-INFERNO+HDI in regions such as TENA, NHAF, and SHAF have a greater impact on the global metrics than the reduced performance seen for regions such as CEAM, NHSA, SHSA, EURO, and MIDE. For regions such as BOAS, CEADS, SEAS, EQAS, and AUST, both model configurations underperform in terms of standard deviation, and any differences between the  $STD / STD_{GFED4s}$  are small when compared to the observed standard deviation (e.g., difference between the JULES-INFERNO and JULES-INFERNO+HDI  $STD / STD_{GFED4s}$  smaller than 15%).

Furthermore, for some of these regions INFERNO is not expected to agree well with observations, especially in terms of variability, as the fire behaviour of some of these regions is characterised by mechanisms that are not represented in INFERNO. This will be further discussed in Section 4.

### 3.3 Impact on burnt area trends

~~Including~~ Representing the socio-economic factors through HDI in INFERNO adds a new external constraint to the model. Through this, historical changes to socio-economic factors influence how changes in population density affect fire ignitions

in the model (see Section 2.3 and Figure 4). Specifically, for regions with high HDI, variations in population have less of an impact on anthropogenic ignitions, while for regions with low HDI, variations in population can have a more considerable impact. This alters the importance of population density changes for highly developed regions, making HDI the dominant factor shaping burnt area trends.

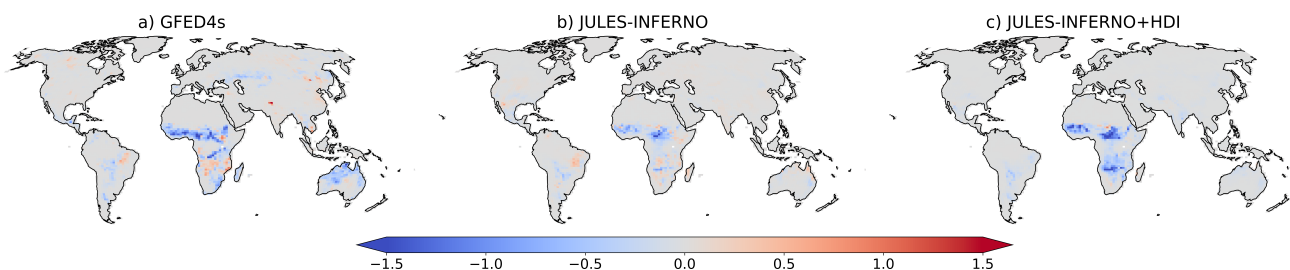


**Figure 13.** Burnt area fraction trend ( $\% \text{ year}^{-1}$ ) (calculated between the period 1997 - 2016) for a) GFED4s, b) JULES-INFERNO and c) JULES-INFERNO+HDI.

615 As shown in Figure 13, both JULES-INFERNO and JULES-INFERNO+HDI represent the main global burnt area trends. JULES-INFERNO is able to represent the regions with burnt area increases (e.g., Southern Africa and Northeast South America) and captures the dominant region for decreased burnt area - North Africa. However, this model setup tends to have weaker negative trends when compared to GFED4s. Conversely, JULES-INFERNO+HDI presents stronger trends, better representing those found in observations. However, it does not reproduce the positive trends in Southern Africa and Northeast  
620 South America. Both JULES-INFERNO and JULES-INFERNO+HDI are unable to represent the observed trends in Central Asia or Boreal North America.

Nonetheless, it should be noted that over the 2001–2012 period, Andela and Van Der Werf (2014) estimated that 51 % of the upward trend over southern Africa can be attributed to El Niño-Southern Oscillation (ENSO), while there is also evidence that socio-economic developments can be responsible for a decline. The relation between ENSO and annual burned area depends  
625 both on the effect of ENSO on precipitation and on the antecedent precipitation-burned area response. While the model setup is able to capture ENSO variability, as its weather is driven by reanalysis, there is no mechanism that allows INFERNO to represent the antecedent precipitation-burned area effects due to litter build up. This is a limitation of the model and it should not be expected for the model to perform well in regions where this precipitation-burned area coupling can be dominant, such as Central America, Northern Hemisphere South America, Europe, Northern Hemisphere Africa, and Central Asia (Andela  
630 et al., 2017; Abatzoglou et al., 2018).

Overall, including-representing the socio-economic factors through HDI in INFERNO results in an improvement in burnt area trends in comparison with observations. As seen in Table A1, JULES-INFERNO+HDI better represents the global negative trend in burnt area when compared to observations ( $-6.77 \text{ Mha\_year}^{-1}$   $\text{Mha\_year}^{-1}$  for GFED4s,  $-2.24 \text{ Mha\_year}^{-1}$   $\text{Mha\_year}^{-1}$  for JULES-INFERNO, and  $-7.58 \text{ Mha\_year}^{-1}$   $\text{Mha\_year}^{-1}$  for JULES-INFERNO+HDI). This improvement comes  
635 mostly from a better representation of the burnt area trends in regions with strong negative trends, such as SHSA, NHAf,

CEAS and AUST, but also by better representing regions with weak negative burnt area trends, namely CEAM, NHSA, EURO and BOAS. Moreover, in regions such as CEAM, NHSA, EURO, BOAS, CEAS, and AUST, JULES-INFERNO+HDI shows a negative burnt area trend, in better agreement with observations.

640 Contrary to these improvements, JULES-INFERNO+HDI can also produce trends that are too strong, reflecting the presence  
of compensating biases in the model. For example, ~~for in~~ Southern Hemisphere Africa (SHAF), although JULES-INFERNO+HDI  
~~has the same reproduces the observed negative~~ burnt area trends ~~sign as in the observations (negative), the trend is too strong~~  
~~(-0.54 Mha year<sup>-1</sup>, the magnitude of the trend is substantially overestimated (-0.54 Mha year<sup>-1</sup> for GFED4s, -0.14 Mha year<sup>-1</sup>~~  
~~-0.14 Mha year<sup>-1</sup> for JULES-INFERNO, and -1.94 Mha year<sup>-1</sup>-1.94 Mha year<sup>-1</sup> for JULES-INFERNO+HDI), and~~. In  
this region, the improved agreement in the sign of the trend in JULES-INFERNO ~~provides a better representation in these~~  
645 ~~regions. In addition, for regions where observations show a positive burnt area trend (TENA, MIDE and SEAS), +HDI arises~~  
from compensating biases that mask an excessive sensitivity to human influence, whereas JULES-INFERNO provides a more  
realistic representation of the trend magnitude. This example highlights that, as for JULES-INFERNO, apparent improvements  
in some metrics in JULES-INFERNO+HDI ~~has a trend of opposite sign (negative). At the same time, JULES-INFERNO can~~  
~~capture the positive trend in TENA and SEAS, such as regional or global trends, can result from compensating errors rather~~  
650 than an overall improvement in process representation.

Nonetheless, the observed dataset (GFED4s) shows that out of 14 regions, four have positive burnt area trends (Table A1). JULES-INFERNO only presents a positive trend for TENA and SEAS. While JULES-INFERNO+HDI tends to enforce decreasing trends, this only happens in four regions out of 14 (i.e., TENA, SHAF, MIDE, and SEAS). For the remaining 10  
655 GFED4s.

It should be noted that, in some of these regions INFERNO does not model all the processes that represent fire behaviour. This has an impact on overall model results. For example, due to the typical model resolution and timescales in Earth System Modelling, INFERNO was not designed to model the processes and mechanisms that are needed to represent large and severe fires which dominate the trends and fire regime characteristics of these regions. Therefore, it is expected that regions where fire  
660 regimes are dominated by large and severe fires may be affected by a negative bias in burnt areas and fire emissions, as well as on their response to a changing climate.

### 3.3.1 Impact of external model drivers on burnt area trends

As described in section 2.4, the JULES-ES experimental setup relies on ancillary forcing data to represent external processes to JULES, such as atmospheric weather conditions, atmospheric composition, population density, and biogenic drivers. These  
665 external forcings can drive fire by forcing changes to the evolution of land surface properties, fire ignitions, and fire weather. It is important to understand the impact these external drivers have on the burnt area trends and the interaction with the parametrised socio-economic factors in fires. Therefore a set of sensitivity experiments was performed by fixing the external model drivers to the year 1990 and only allowing an individual external driver to vary transiently through the experiment.

- **1990 control:** where all external model drivers are fixed to year-1990 values
- 670 – **clim:** where only the atmospheric drivers are transient (downward longwave radiative flux, downward shortwave radiative flux, precipitation, surface pressure, air temperature, meridional and zonal wind components)
- **tas:** where only air temperature at 2 m is transient
- **ppn:** where only precipitation is transient
- **lu:** where only the land use is transient
- 675 – **Ndep:** where only Nitrogen deposition is transient
- **pop:** where only population density is transient
- **CO<sub>2</sub>:** where only the atmospheric carbon dioxide (CO<sub>2</sub>) mixing ratio is transient
- **HDI:** where only the Human Development Index is transient (only for JULES-INFERNO+HDI)

These sensitivity experiments branched from their respective control runs - JULES-INFERNO and JULES-INFERNO+HDI  
 680 - starting from 1990 and run up to 2016. In this way, the underlying land surface state from the reference run is preserved, and only changes to the forcing that take place during the period of interest are taken into effect. The trends for each relevant external forcing are in Supplementary Figure A2.

The results of these sensitivity experiments on the burnt area trends ( $Mha\ year^{-1}$ ), and respective standard error, for the different GFED4s fire regions are presented in Table A2 in the Appendix for JULES-INFERNO and Table A3 for JULES-  
 685 INFERNO+HDI. These results are summarised in Figure 14. Burnt area trends in JULES-INFERNO tend to be driven by climate, land use, or population density changes (relative contribution greater than 50 % when compared to their reference), with the dominant driver (the sensitivity experiment with the largest absolute trend value) for the majority of regions being climate (including through air temperature and precipitation), for example, BONA, TENA, NHSA, SHSA, EURO, MIDE, SHAF, BOAS, CEAS, SEAS, and AUST. On the one hand, air temperature is a dominant, and statistically significant, driver of  
 690 increasing burnt area trends for CEAM, NHSA, BOAS and CEAS. For MIDE, precipitation has a dominant role in reducing burnt area. On the other hand, despite dominating the burnt area trends, temperature ~~and precipitation~~ can have opposite effects. Namely, for ~~BONA (not significant for air temperature), TENA , SHSA, EURO , and AUST, precipitation causes a reduction in burnt area, while where~~ temperature results in an increase ~~, although results are not statistically significant for precipitation over TENA, SHSA, EURO, CEAS, CEAM and AUST~~ in the trend.

695 Anthropogenic drivers, such as land use and population density can play a major role in some regions. For example, land use is the dominant driver in SHSA and SHAF, population density in CEAM, and both are important drivers in TENA, EURO, MIDE, NHAF. Land use can cause either an increase (TENA, EURO, and SHAF) or a decrease in burnt area, while population density results in a reduction in burnt area for all the regions where this external driver is dominant (TENA, CEAM, EURO, MIDE, and NHAF).

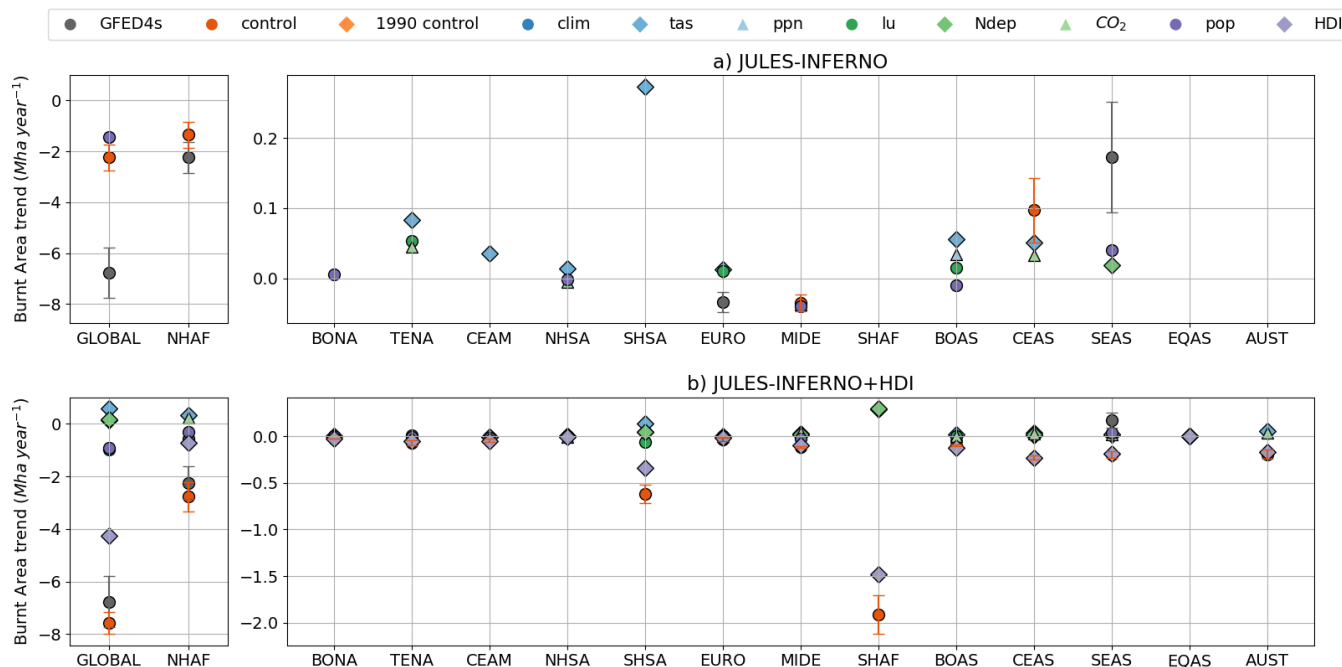


**Figure 14.** Burnt area trends ( $Mha \cdot year^{-1}$ ) for the different GFED4s fire regions (Giglio et al., 2013) from the model sensitivity experiments for a) JULES-INFERNO and b) JULES-INFERNO+HDI. Only trends that are statistically significant at the 95 % confidence level are shown. The whiskers for the values of GFED4s and *control* represent the standard error associated with the trend. Markers whose edge is coloured in black represent trends that are significantly different from zero at the 99 % confidence level. GLOBAL and NHAF regions are presented in separate panels to improve readability, due to their large trends compared to other regions.

700 Biogenic drivers such as nitrogen deposition and atmospheric carbon dioxide assimilation tend to play a less significant role in the burnt area trends, impacting burnt area trends only for NHSA through carbon dioxide, and CEAS through both nitrogen deposition and atmospheric carbon dioxide.

For JULES-INFERNO+HDI, HDI is the dominant factor in the burnt area trend for all regions, with the exception of NHAF and EQAS. This is evident in the sensitivity experiments for JULES-INFERNO+HDI where only HDI forcing is made transient  
 705 (*HDI*). In all cases, including representing the socio-economic factors through HDI in INFERNO changes the relative role that external forcings have in determining burnt area trends. For example, it reduces the role that climate, population density, and land use have in burnt area trends towards a stronger role from socio-economic effects (*HDI*).

This impact is especially evident when comparing the role of the climate forcing in driving burnt area trends between JULES-INFERNO and JULES-INFERNO+HDI in their respective sensitivity experiments, *clim*, *tas*, and *ppn*. For instance,  
 710 for regions where temperature effects on burnt area trends were dominant in JULES-INFERNO, they show less of an impact from temperature in JULES-INFERNO+HDI, albeit still at a statistically significant level (e.g., TENA, EURO, CEAS, and AUS). In addition, where the climate contributions to the burnt area trends were small in JULES-INFERNO (BONA, CEAM,

and NHTS), when considering socio-economic factors, these become statistically non-significant in terms of the climate contributions to the trends. In addition, ~~including-representing the~~ socio-economic factors through HDI in INFERNO leads to a change in how precipitation and temperature can impact some regions. For example, precipitation was the dominant driver of burnt area trends in JULES-INFERNO for MIDE, causing a reduction of burnt area (trend of  $-0.038 \text{ Mha year}^{-1}$ ). Conversely, in JULES-INFERNO+HDI, precipitation has less impact on the burnt area trend (trend of  $-0.016 \text{ Mha year}^{-1}$ ), while temperature has a larger impact on the burnt area trend ( $+0.034 \text{ Mha year}^{-1}$ ). A similar result is also seen for NHTS, where the role of temperature becomes statistically significant in JULES-INFERNO+HDI (trend of  $+0.342 \text{ Mha year}^{-1}$ ); ~~while it was not statistically significant in JULES-INFERNO (trend of  $+0.007 \text{ Mha year}^{-1}$ ).~~

Moreover, results show a difference in the role of anthropogenic drivers (land use and population density) on burnt area trends between JULES-INFERNO and JULES-INFERNO+HDI sensitivity experiments. For BONA, CEAM, and NHTS regions, burnt area decreases for JULES-INFERNO+HDI (*pop* and *lu*) sensitivity experiments while for JULES-INFERNO (*pop* and *lu*) an increase was simulated.

Together, these results ~~show that including-indicate that representing~~ socio-economic factors ~~in the representation of fires in Earth System Models is important for simulating the burnt area mean state, for quantifying burnt area trends and for understanding the main drivers of those~~ through HDI can influence the simulation of burnt area in ESMs, but that its impact is regionally heterogeneous and involves clear trade-offs. The inclusion of HDI in JULES-INFERNO primarily improves the mean-state representation and trend magnitude in regions where the original model exhibits strong positive biases. However, these improvements are not uniform across all fire regions. In several regions the additional constraint imposed by the use of HDI as a proxy for socio-economic impacts on fire leads to reduced variability or amplified negative biases. Overall, JULES-INFERNO+HDI demonstrates that socio-economic development can be an important modulator of fire activity and trends at regional scales, but further refinement of JULES-INFERNO+HDI is still required to better balance its effects across different fire regions.

#### 735 4 Discussion & Conclusions

This work aims to represent socio-economic factors, through the use of the HDI, together with the Pechony and Shindell (2009) anthropogenic fire ignitions to parameterise human socio-economic impacts on fires. When using the INFERNO fire model, the aim was to improve the regional representation of human–environmental coupling for applications at large spatial scales within an ESM.

The results presented in this study ~~show that including-indicate that incorporating~~ socio-economic factors through HDI in the fire ignition and suppression parametrisation within INFERNO ~~together with,~~ alongside the revised  $\overline{BA_{PFT}}$  parameters, ~~leads to an improved-can improve the~~ representation of the globally-averaged linear relationship between burnt area and HDI, as ~~found in observations--observed in~~ Figures 3 and 6 ~~leading in turn to improvements in.~~ This adjustment leads to better performance in regions ~~that were affected by where~~ JULES-INFERNO previously exhibited large positive biases ~~in the JULES-INFERNO configuration. However, the improvements are regionally variable, and in some areas the inclusion of~~

HDI introduces trade-offs, such as reduced variability or less accurate representation of small to moderate fires, highlighting the need for further refinement of the approach.

The simple representation of HDI captures how more complex socio-economic processes tend to suppress fires as development increases. ~~The observed linear~~ In our analysis, we modelled the relationship between burnt area and HDI using a linear form  
750 for simplicity. It is important to note that this does not imply that the relationship is inherently linear in the observed data. This result should be interpreted as conditional on the linear model; it reflects a statistical trend rather than a directly observed linear relationship.

This approach suggests that regions with higher HDI tend to have lower average values of burnt area. This trend can be attributed to various components of HDI that influence government policies and resources for fire management (Miranda-  
755 ~~Lescano et al., 2023). For instance, the gross national income index indicates that higher HDI regions typically have more funding available for fire prevention and suppression efforts (Rideout et al., 2017). Similarly, the life expectancy index suggests that these governments are more likely to implement policies aimed at mitigating the negative impacts of fire on their population (Rizzo and Rizzo, 2024)~~income component of HDI broadly reflects economic capacity, which can affect the ability to resource wildfire management; accordingly, Rideout et al. (2017) illustrate how strategic budgeting and planning tools (e.g., STARFire)  
760 can be used to allocate limited resources across preparedness and fuel treatment programmes based on risk, valuation, and cost information. Rizzo and Rizzo (2024) highlight that wildfire smoke has substantial adverse health impacts and therefore motivates mitigation and adaptation actions (e.g., risk communication and preparedness/early-warning measures) aimed at reducing exposure and protecting vulnerable populations. Additionally, the education ~~index highlights that educational initiatives can enhance community~~ component of HDI may be relevant because public awareness and preparedness ~~regarding fire risks and environmental stewardship (Prestemon et al., 2010).~~ can influence fire risk; for example, a Florida case study found that wildfire prevention education efforts (e.g., public service announcements and outreach) were associated with fewer preventable human-caused ignitions across several ignition categories (Prestemon et al., 2010).

Collectively, these factors help explain the observed trend and underscore the utility of HDI as a general proxy for representing socio-economic influences in fire management, but may not be fully representative of specific particularities of any single given  
770 region.

Large bias reductions are evident in Temperate North America (TENA), Central America (CEAM), Southern Hemisphere South America (SHSA), Europe (EURO), and Middle East (MIDE), with the largest reductions in TENA where a 735.57 % bias in JULES-INFERNO is reduced to 44.46 % in JULES-INFERNO+HDI. It should be noted that for Australia and New Zealand (AUST) and East Asia ~~Asia~~ (SEAS), JULES-INFERNO+HDI performance is ~~reduced~~ degraded, increasing the  
775 negative bias ~~when compared to INFERNO-JULES. Furthermore, it should be highlighted that compared to JULES-INFERNO.~~ JULES-INFERNO includes contributions from regions with large positive biases exceeding +150 % (TENA, CEAM, SHSA, EURO, and MIDE), with a combined bias of +76.96 Mha (Table A1). These are the regions targeted for bias reduction in JULES-INFERNO+HDI. Considering that JULES-INFERNO's overall global bias is -34.35 Mha, removing the compensating effect of these highly biased regions would imply a potential global bias of approximately -111.31 Mha. This highlights the  
780 importance of addressing regional biases and demonstrates that although JULES-INFERNO ~~performs~~ appears to perform well

at the global scale, ~~as can be~~ as seen when comparing ~~the~~ annual mean burnt area against GFED4s in Figure 12, this is largely due to compensating errors at the regional level.

The histograms of burnt area frequency across different fire regions, ~~Figure 10,~~ (Figure 10) reveal key differences in how fire sizes are distributed between JULES-INFERNO, JULES-INFERNO+HDI, and GFED4s observations. The implementation  
785 of HDI ~~resulted in notable~~ leads to improvements in regions such as Temperate North America (TENA), Central America (CEAM), and Southern Hemisphere South America (SHSA), and where reductions in the frequency of large fires correct strong overestimations present in JULES-INFERNO. In other regions, such as Northern Hemisphere Africa (NHAF). ~~In these regions, the reduction in the frequency of large burnt areas suggests that including socio-economic factors better captures the dynamics of fire suppression associated with higher levels of human development and management practices. However, discrepancies against observations remain in JULES-INFERNO+HDI for regions such as,~~ the inclusion of HDI further suppresses medium to large fires, but this does not consistently improve agreement with observations. In Northern Hemisphere South America (NHSA), ~~and~~ Australia and New Zealand (AUST), ~~where the model continues to underpredict~~ the underprediction of medium and large fire sizes in JULES-INFERNO further degrades with the inclusion of HDI, highlighting the regional trade-offs associated with the socio-economic parametrisation.

795 Moreover, ~~including representing the~~ socio-economic factors through HDI in INFERNO-JULES+HDI improves the representation of the burnt area trends, especially in areas where GFED4s presents negative trends. At the same time, JULES-INFERNO shows no significant trends (e.g., SHSA, NHAF, CEAS, and AUST), as well as better representing regions with weak negative burnt area trends (CEAM, NHSA, EURO, and BOAS). However, JULES-INFERNO+HDI can also produce overly strong trends (e.g., SHAF) or misrepresents the observed positive burnt area trends found in TENA, MIDE, BONA, and SEAS.

800 As mentioned previously, observations (GFED4s) show that out of 14 regions, four have a positive burnt area trends. From these, only JULES-INFERNO shows a positive trend for TENA and SEAS. While JULES-INFERNO+HDI tends to strengthen decreasing trends, this only happens in four regions out of 14 (TENA, SHAF, MIDE, and SEAS). For the remaining 10 regions, JULES-INFERNO+HDI shows a similar trend to JULES-INFERNO or even an improved trend when compared to GFED4s.

It should be highlighted that in some of these regions, INFERNO does not model all of the processes that impact fire  
805 behaviour. This has an impact on overall model results. For example, INFERNO was not designed to capture the dynamics of large, severe fires that dominate fire regimes in some regions. As a result, these areas may show a negative bias in burned area and fire emissions, as well as in their response to climate change.

Overall, the improved representation of the burnt area trends in JULES-INFERNO+HDI when compared to JULES-INFERNO highlights the importance of including the socio-economic factors in fire ignition and suppression in order to better reproduce  
810 the observed fire trends. This impact is especially evident when comparing the role of external climate drivers on burnt area trends between JULES-INFERNO and JULES-INFERNO+HDI using a set of sensitivity experiments. The results of these experiments show that including socio-economic impacts on fire results in the burnt areas trends being dominated by socio-economic drivers through a reduction in the contribution from climate drivers, especially from temperature and precipitation.

## 4.1 Modelled burnt area trends

815 We have shown that introducing the representation of socio-economic factors can change the impact external forcing has on  
burnt area trends and that the mechanisms that lead to this can differ at a regional level. For example, the inclusion of socio-  
economic factors reduces the role of temperature in driving trends (e.g., increase for TENA, EURO, CEAS, and AUS), as well  
as by changing the behaviour that climate drivers have in burnt area trends (e.g., MIDE, NHAF, and SEAS). Socio-economic  
factors also alter the influence of land use and population density, increasing their impact on fire activity by shaping how human  
820 activity interacts with fire regimes. (e.g., BONA, CEAM, and NHSA).

Although HDI does not ~~encompass explicitly~~ explicitly encompass the impacts of fire management policies, these results are  
consistent with ~~other studies, which show that~~ for previous studies demonstrating that, in highly developed regions, ~~land and fire~~  
~~management policies have a greater role than other human behaviours in controlling ignitions~~ (Nikolakis and Roberts, 2022; Ford et al., 2022)  
institutional capacity and land-management policies exert a stronger control on fire activity than individual ignition behaviours.  
825 For example, Carreiras et al. (2014) show that in Mediterranean Europe, changes in land management and fire suppression  
policies have contributed to declining burnt area despite sustained human presence. Mourão and Martinho (2014) highlight the  
role of coordinated public policies and investment in fire prevention and suppression infrastructure in reducing fire impacts in  
developed regions. Ford et al. (2021) demonstrate that governance quality and fire management strategies, rather than ignition  
pressure alone, are key determinants of fire outcomes in high-income countries. Similarly, Jacobson et al. (2022) find that  
830 institutional fire management capacity strongly moderates the relationship between human activity and fire occurrence. Finally,  
Nikolakis and Roberts (2022) emphasise the importance of governance structures and policy frameworks in shaping fire regimes,  
showing that effective land and fire management institutions can substantially limit fire extent even under increasing anthropogenic  
pressure.

The work of Kelley et al. (2019) and Jones et al. (2022) shows that, despite the increases in fire weather seasons and fire  
835 weather extremes that have been observed in all world regions, burnt area has shown a variety of regional trends and that the  
negative trends were found to be significant only in Africa (NHAF and SHAF), Europe (EURO), and Central Asia (CEAS). At a  
global scale, burnt area trends show a decline predominantly driven by a decline in burnt area in the savannah-grassland systems  
caused by the expansion of high-capital agriculture (Andela et al., 2017), as well as reductions in vegetation productivity driven  
by changes to the hydrological balance (Zubkova et al., 2019). The results on the impact of external model drivers on burnt  
840 area trends, detailed in Section 3.3.1, agree with this. In both JULES-INFERNO and JULES-INFERNO+HDI, the dominant  
factor contributing to the negative trend in global burnt area are linked to anthropogenic drivers (land use, population density  
and HDI), as well as precipitation. ~~Several authors have also~~

Several studies have shown that declines in burnt area ~~in-across~~ the Mediterranean have occurred ~~irrespective of~~ despite  
increases in fire weather ~~, as well as extensions to severity and extensions of the fire weather season length, which is attributed~~  
845 ~~to increased fire prevention and in combating and,~~ with these declines largely attributed to enhanced fire prevention, suppression  
capacity, and fire management strategies. For instance, (Rabin et al., 2017) demonstrate that improvements in suppression  
efficiency and fire management practices have offset the effects of increasingly severe fire weather in Mediterranean Europe.

(Jones et al., 2022) show that trends in burnt area are weakly coupled to fire weather in recent decades, highlighting the dominant role of human intervention in limiting fire spread. Similarly, (Carreiras et al., 2014) attribute declining burnt area to changes in land management and fire suppression policies rather than to climatic drivers alone. In addition, (Mourão and Martinho, 2014) emphasise that increased investment in fire prevention and coordinated policy responses have been critical in mitigating fire impacts (Jones et al., 2022; Urbietta et al., 2019; Carreiras et al., 2014; Mourão and Martinho, 2014) despite a lengthening fire season.

Moreover, results show the impact of the anthropogenic drivers (land use and population density) have in the burnt area trends, resulting in a decrease in burnt area for JULES-INFERN0+HDI compared to JULES-INFERN0, for BONA, CEAM, and NHSA regions. This result, combined with the impact seen in the reduction of the effects temperature has in burnt area, are especially relevant in South America (NHSA and SHSA), leading to a better performance of JULES-INFERN0+HDI in these regions overall. The impact of socio-economic effects on fire is also well documented for the Amazonia region, where fire is routinely used for land clearing, resulting in a strong link between burnt area and deforestation rates. Through and is tightly linked to deforestation rates (Silva Junior et al., 2021). Over the last decade, this region has seen a decline in deforestation rates leading to owing to policy interventions and regulatory enforcement have led to an observed negative trend in burnt area overall burnt area (Nepstad et al., 2014). However, this decline in burnt area has not been uniform due to, as drought-related fire incidence has sometimes increased even when deforestation slowed, reflecting historical shifts in economic conditions and environmental policies (Silva Junior et al., 2021; Aragão et al., 2018; Nepstad et al., 2014) (Aragão et al., 2018).

The analysis of the impact of including representing the socio-economic factors through HDI in INFERN0 has also shown that JULES-INFERN0+HDI can also producing overly strong negative trends resulting in worse performance when compared to JULES-INFERN0 (e.g., SHAF). In addition, for regions where observations present a positive burnt area trend (TENA, MIDE and SEAS), JULES-INFERN0+HDI presents an opposite trend sign (negative), while JULES-INFERN0 is able to capture the positive trend in TENA and SEAS.

It is known that there is an increase in the frequency of large and severe fires in Continental United States of America (Goss et al., 2020; Williams et al., 2019; Abatzoglou and Williams, 2016), as well as boreal regions (Canada and Alaska) (Kasischke and Turetsky, 2006; Stocks et al., 2002; Veraverbeke et al., 2017), leading to observed increases in burnt area, with fire activity having a strong relationship with fire weather in these regions.

However, INFERN0 has been developed for Earth System Modelling resolutions and timescales, and it is not expected to be able to capture the representation of the processes. While ESMS can, in principle, represent fire spread using more detailed fire modules (e.g., Lasslop et al., 2014), INFERN0's current implementation relies on the average burnt area for each PFT ( $\overline{BA_{PFT}}$ ) formulation in Eq. 5. This approach does not capture the fine-scale dynamics that drive large and severe fires which dominate the trends and fire regime characteristics of these regions (e.g., it is based on the use of a value for the average burnt area for each plant functional type). Therefore, it is expected that, meaning that INFERN0 may underestimate both the occurrence and extent of extreme fire events. Even in models that explicitly represent fire spread, the ability to resolve these dynamics is constrained by the spatial and temporal resolution at which the ESM is run. Consequently, regions where fire

regimes are dominated by large and severe fires may be-affected-by-experience a negative bias in predicted burnt areas and fire emissions, as well as on-their-in-their-simulated response to a changing climate.

## 885 4.2 Model limitations and known issues

The use of socio-economic factors in INFERNO reduces the inter-annual variability of burnt area for most of the fire regions (Figure 11). While this improves INFERNO performance over regions such as TENA and CEAM, it results in a reduction in the variability overall, reducing the ability of the model to represent the burnt area regions that are characterised by high inter-annual variability, namely, BONA, BOAS, AUST, CEAS, SHSA and NHSA. Although this could-be-seen-as-a-negative  
890 impact further-exacerbates-the-under-estimation-of-inter-annual-variability-in-JULES-INFERNO+HDI, it must be noted that the control model - JULES-INFERNO - despite having a larger inter-annual variability, also underperforms in this aspect compared to observations.

Although socio-economic factors are included in JULES-INFERNO+HDI, the HDI dataset provides information mainly at a national level. To improve the impact of socioeconomic activities on fire at a regional level, it would be beneficial to use data  
895 capturing the HDI changes at a sub-national administrative level. Furthermore, it should be highlighted that the HDI does not account for the different implementation of fire management practices and government policies at the regional level.

Another limitation in the representation of fires in INFERNO is the lack of a peat-burning in the model simulations described here. The work of Teixeira et al. (2021) highlights that this could be responsible for the negative bias over equatorial Asia and boreal regions where peatland fires represent a significant amount of burnt area and biomass burning emissions. Recent  
900 developments from Blackford et al. (2024) could significantly improve the model performance over these regions and help to reduce the burnt area bias both at regional and global scales.

It should be noted that, INFERNO represents burnt area as the average per fire for each PFT, decoupling fire spread from localised influences such as wind, weather variability, and topography. This allows the model to capture broad-scale, climate and vegetation-driven fire dynamics through PFT-specific flammability and fire occurrence metrics. However, sub-grid  
905 heterogeneity in terrain or meteorology is not explicitly resolved, which may lead to under-representation of local-scale fire spread and associated impacts.

In addition, biases in the underlying vegetation can significantly impact modelled burnt area. For example, (Forkel et al., 2019) demonstrated that many global fire models exhibit widespread shortcomings in capturing the sensitivity of burnt area to vegetation characteristics such as leaf area index and plant productivity. Such biases can propagate through modelled fire  
910 dynamics, leading to systematic over or underestimation of burnt areas, particularly in regions where vegetation structure strongly regulates fuel availability. The work by Teixeira et al. (2021) is a good example of this. In their work, the authors show that although the burnt area fraction over Africa is well represented, there is a large (50 %) underestimation of the fires in the northern African region (NHAF). This underestimation is attributed to the Saharan bare soil extending too far south, causing a lack of grassland in the Sahel region, which is a result of precipitation deficits associated with errors in the position  
915 and intensity of monsoon systems (Sellar et al., 2019b; Williams et al., 2018).

Despite the improvements introduced by Burton et al. (2019) to JULES, including fire-vegetation interactions, there are still a number of regions that show significant vegetation biases, which in turn affect the performance of INFERNO. For example, ~~it is known~~ (Burton et al., 2019) shows that JULES vegetation has few needle-leaf trees across the boreal regions compared to observations.

920 These results highlight that the high burnt area variability in these regions may result from a mechanism not currently represented in INFERNO. For example, Kirillina et al. (2020); Andela and Van Der Werf (2014) show how changes in areas with increasing anthropogenic alteration, such as agricultural systems, and changes in fire management practices and government policies, often lead to shifts in peak fire activity for regions such as India and southwest Russia. They also show that the widespread adoption of Aboriginal fire management with increased prescribed burning has curbed the frequency of  
925 large fires over a broad region in Australia. Similarly, the dominant spatial and temporal variability in the burnt area for Southern Europe and North Africa (Chergui et al., 2018), as well as South America (Chuvieco et al., 2021), is known to be driven by shifts in the amounts of fuel and continuity imposed by changes in socioeconomic drivers.

### 4.3 Concluding remarks

Socio-economic policies on management and control of fire play a major role in controlling fire ignition and suppression  
930 (Nikolakis and Roberts, 2022; Ford et al., 2021; Jacobson et al., 2022; Carreiras et al., 2014; Mourão and Martinho, 2014). This is especially important in the context of future climate projections (Pivello et al., 2021; Duane et al., 2019; Gillson et al., 2019; Paveglio et al., 2018). It is only with the understanding of the expected impact of climate change that adaptation and mitigation policies can be developed with the aim of protecting infrastructure and ecosystems from fire hazards. This shows the importance of representing socio-economic controls on fire when modelling future projections in an Earth System Modelling  
935 context.

This study shows that including a parametrisation for socio-economic impacts on fire based on HDI in INFERNO provides a simple ~~and linear representation~~, linear approximation of these effects on fire ignition and suppression. This ~~leads to an improvement in model performance, especially in developed regions~~ approach improves the representation of regions where JULES-INFERNO exhibits large positive biases, such as TENA, CEAM, SHSA, EURO, and MIDE. However, the improvements are regionally variable, and in some areas the inclusion of HDI can reduce variability or exacerbate negative biases, highlighting the trade-offs associated with this simplified socio-economic parametrisation.  
940

Introducing socio-economic factors into INFERNO ~~reduces compensating biases and improves the modelled burnt area trends in comparison with observations in several regions.~~ In particular, the results here show that ~~including representing the socio-economic factors through HDI in the representation of fires in Earth System Models is important for realistically simulating ESMs can help simulate the burnt area mean state, for quantifying burnt area trends in the recent past, and for understanding the main drivers of those trends more realistically, quantify recent past trends, and the relative importance of socio-economic versus climatic and population drivers~~ at regional scales. ~~However, these improvements are not uniform, and in some regions the inclusion of HDI can dampen variability or amplify existing negative biases, highlighting the limitations of a simple, globally applied socio-economic proxy.~~  
945

950 The improvements seen in JULES-INFERNO+HDI ~~has in for~~ regions such as TENA, NHAF, and SHAF ~~have a greater impact in the~~ contribute more strongly to global metrics than the reduced performance ~~seen for~~ observed in regions such as CEAM, NHSA, SHSA, EURO, and MIDE. ~~For~~ However, in regions such as BOAS, CEADS, SEAS, EQAS, and AUST, both model configurations underperform in ~~terms of standard deviation and any representing variability, and the~~ differences between the modelled and observed standard deviation (STD / STD<sub>GFED4s</sub> are small when) remain relatively small compared to  
955 the observed ~~standard deviation variability~~ (e.g., ~~difference between the differences between~~ JULES-INFERNO and JULES-INFERNO+HDI STD / STD<sub>GFED4s</sub> are generally smaller than 15 %). These results highlight that, while the inclusion of HDI can improve global-level metrics, regional performance remains heterogeneous and some limitations in capturing sub-annual variability persist.

For regions such as NHSA, BOAS, CEAS, and AUST there is an increase in the bias introduced. However, it should be noted  
960 that these model limitations and known issues are discussed in Section 4.2 where the limitations of the model are highlighted and related to fire mechanisms that are not represented in INFERNO, or bias in the underlying vegetation model causing impacts on the modelling of fires. In future work, incorporating processes such as fire intensity, fuel type, seasonal timing, and vertical extent would be required for a more mechanistic representation of emission injection and atmospheric transport, and may lead to improvements in the model.

965 Finally, the recent work by Perkins et al. (2024), proposes an alternative methodology for representing human influences in INFERNO. While the WHAM! framework introduced by Perkins et al. (2024) offers a more comprehensive approach, its increased complexity may present challenges in implementation within an ESM context. In contrast, the method presented in this study is straightforward and is directly applicable within the existing modelling framework of JULES-INFERNO for ESM.

Considering this, we recommend that socio-economic factors should be included in all fire modelling studies at both global  
970 and regional scales, particularly when considering future climate change scenarios. This work will form the basis of a future study on understanding the impact of fires in the Earth System when considering future climate change scenarios.

## Appendix A

### A1 Observed Datasets Burnt area evaluation

#### A1.1 The Human Development Index dataset

975 HDI originated from the annual Human Development Reports created by the United Nations Development Programme (UNDP) Human Development Report Office. These reports had the explicit purpose of shifting the focus of development economics from national income accounting to people-centred policies. The aim was to provide a simple composite measure of human development to convince the public, academics, and politicians to evaluate development not only by economic advances but also improvements in human well-being. HDI serves as a crucial metric for assessing the development status of regions globally, and it has been used in several studies to better understand the socio-economics impacts in the Earth System (ES) (Türe, 2013; Hiekel, 2020; Roy et al., 2023).

980 HDI is a composite index (ranging from zero to one) measuring four key metrics (Bhanojirao, 1991) To analyse the model performance, we calculated the following statistical and error measures, relative to the observed (GFED4s) and modelled (JULES-INFERNO and JULES-INFERNO+HDI) burnt area:

- 985
- life expectancy at birth
  - expected years of schooling
  - average years of schooling
  - gross national income (GNI) per capita

990 These metrics are then normalised by their respective maximum value, and HDI is calculated as the geometric mean of life expectancy, education, and GNI per capita, as shown in Eq. 1.

Deviation of the modelled data in relation to observed values:

$$\underline{HDI} \phi'_i = \underline{H_N} \cdot \underline{E_N} \cdot \underline{I_N}^{\frac{1}{3}} \phi_i - \phi_{i,obs} \quad (\text{A1})$$

where  $H_N$  is the normalised life expectancy,  $E_N$  is the normalised arithmetic mean of the two education indices and  $I_N$  is the normalised GNI.

- 995
- Bias, which represents the mean deviation of the modelled data in relation to the observed values.

$$\underline{Bias} = \frac{1}{N} \sum_{i=1}^N \phi'_i \quad (\text{A2})$$

The work conducted by Kummur et al. (2018) introduces gridded global datasets for Gross Domestic Product (GDP) and Human Development Index (HDI), covering a 25-year period from 1990 to 2015 with annual frequency and a spatial

resolution of 5 arc-minutes. This temporal coverage and high-resolution global scope enable comprehensive analyses of trends, patterns, and changes in HDI across diverse regions and timescales.

1000

– The Root Mean Square Error.

$$RMSE = \sqrt{\frac{\sum_{i=1}^N (\phi_i - \phi_{i,obs})^2}{N}} \quad (A3)$$

To produce these datasets, Kummu et al. (2018)s employed a comprehensive approach. For GDP, they utilized both sub-national and national-level data sources. Sub-national GDP data was derived from previous research, while national-level data was sourced from reputable institutions such as the World Bank and the Central Intelligence Agency World Factbook. The HDI dataset was compiled by initially constructing a full national HDI dataset based on data from the Human Development Reports by UNDP. For countries not included in the UNDP reports, independent data sources were utilized, and for missing or outdated data, a methodology involving scaled regional data was adopted.

1005

– The Root Mean Square Error after the removal of a constant bias.

$$RMSE_{UB} = \sqrt{\frac{\sum_{i=1}^N [(\phi_i - \bar{\phi}) - (\phi_{i,obs} - \bar{\phi}_{obs})]^2}{N}} \quad (A4)$$

1010

**A1.1 Burnt Area observation**

– Standard deviation for the modelled - equation A5 - and observed - equation A6 - data.

$$STD = \sqrt{\frac{\sum_{i=1}^N (\phi_i - \bar{\phi})^2}{N}} \quad (A5)$$

Basis regions, as defined in the GFED4s dataset (Giglio et al., 2013):

$$STD_{obs} = \sqrt{\frac{\sum_{i=1}^N (\phi_{i,obs} - \bar{\phi}_{obs})^2}{N}} \quad (A6)$$

1015

We use data from the Global Fire Emission Database version 4 (GFED4s) (Giglio et al., 2013) to understand the relation between HDI and burnt area, as well as to assess the model performance in simulating burnt area. This dataset is provided as a gridded product at a 0.25° resolution. It is derived from a multi-sensor satellite dataset, including satellite databased on active fire detection, and including small fires based on statistical modelling, as detailed in (Randerson et al., 2012). We apply regions defined in the GFED4s dataset to the modelled data to evaluate the results at a regional level (Figure A1).

1020

## A1.1 Fire Weather Index

The work developed by Vitolo et al. (2020) provides an ERA5-based global meteorological wildfire danger dataset based on the Global ECMWF Fire Forecast (Geff) model and the ERA5 reanalysis.

1025 In this dataset the FWI is calculated using meteorological variables (e.g., such as temperature, humidity, precipitation, and wind speed) driven by the ERA5 reanalysis dataset. To accurately represent wildfire conditions at local noon, when fire danger is typically highest, atmospheric fields from ERA5 undergo preprocessing, stitching together hourly forecasts, ensuring that meteorological conditions are representative of 12:00 noon local time around the world.

1030 The Geff model calculates the FWI by modelling fuel moisture response to atmospheric forces at different depths. Three fuel moisture levels are used, representing surface fuels, deeper organic material, and compact fuels, each responding at different rates to changes in weather. These moisture codes are then combined to estimate fire behaviour, such as the rate of spread and fire intensity, providing a comprehensive fire danger index were  $i$  is the temporal index and  $N$  is the number of elements of  $\phi$  considered, and  $\bar{\phi}$  is the constant bias.

The Geff-ERA5 FWI reanalysis dataset is available from 1979 onwards, at a spatial resolution of 28 km. Considering these statistics, a perfect simulation would have the following criteria:

1035 When comparing datasets (modelled or observed) at different grid resolutions, the higher-resolution dataset is re-gridded to the lowest-resolution grid using a first-order conservative area-weighted re-gridding method.

–  $RMSE = 0$

–  $RMSE_{UB} = 0$

–  $bias = 0$

1040 –  $Pearson\ correlation = 100\%$

–  $STD / STD_{GFED4s} = 1$

–  $RMSE / STD_{GFED4s} = 0$

–  $RMSE_{UB} / STD_{GFED4s} = 0$

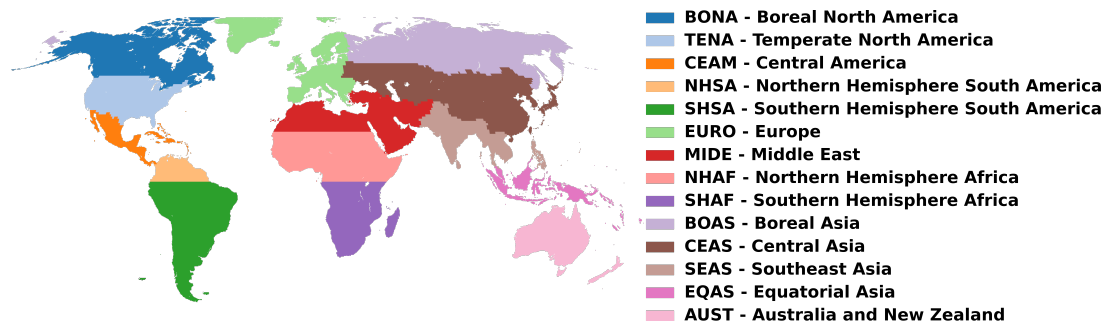


**Figure A1.** Histograms of posterior distributions for Bayesian linear regression fit parameters derived for GFED4s (dashed red line) Basis regions, JULES-INFERNO (dotted green line), and JULES-INFERNO+HDI (solid blue line). Panel a) shows the slope parameter, b) the intercept parameter, and c) depicts the sigma (error term representing random sampling noise) as defined in log-transformed space the GFED4s dataset (Giglio et al., 2013).

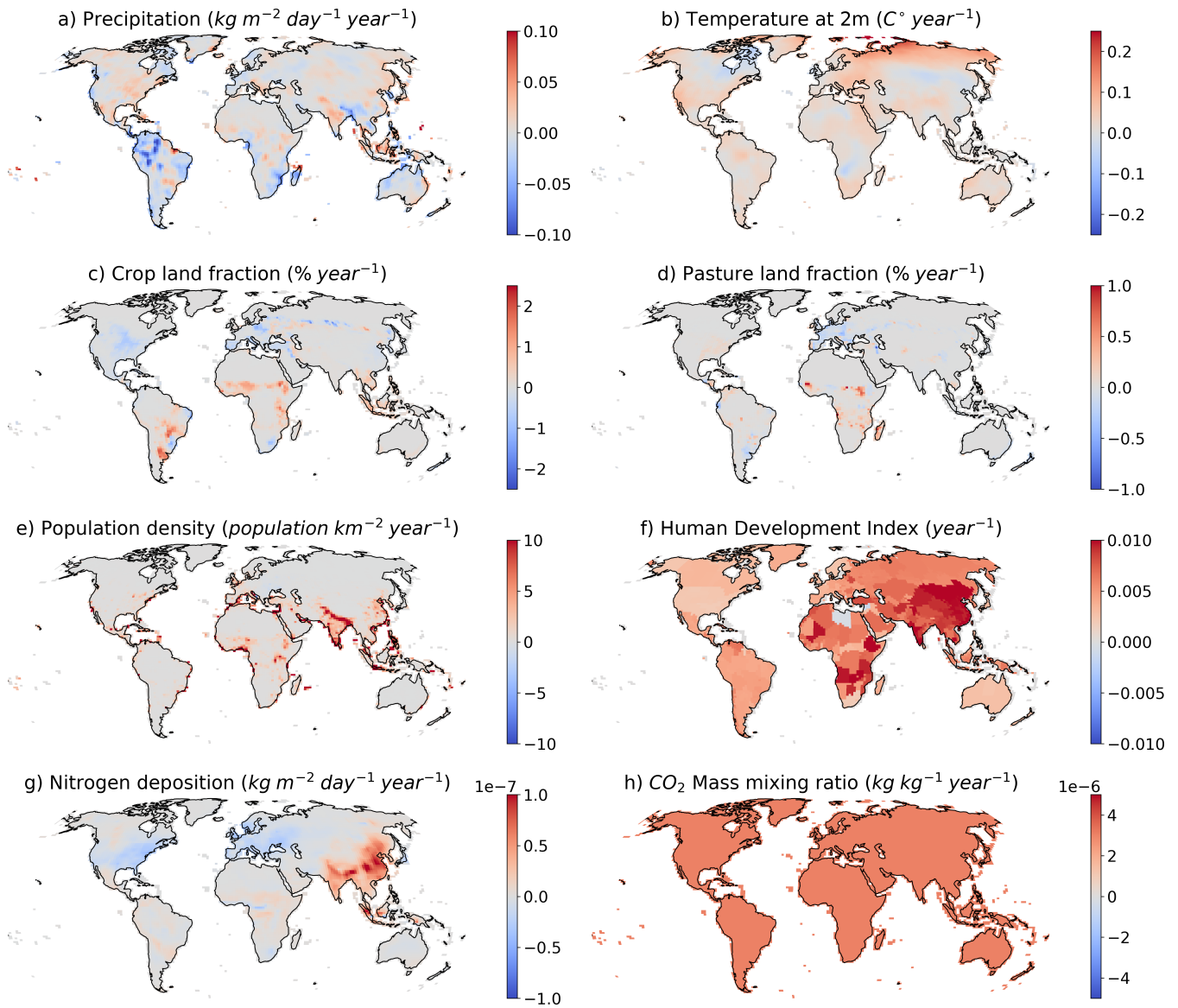


**Figure A2.** Trends calculated between the period 1997 - 2016 for JULES-ES external forcing variables a) Precipitation ( $kg\ m^{-2}\ day^{-1}\ year^{-1}$ ), b) Temperature at 2 m ( $C^{\circ}\ year^{-1}$ ), c) Crop land fraction ( $\%\ year^{-1}$ ), d) Pasture land fraction ( $\%\ year^{-1}$ ), e) Population density ( $population\ km^{-2}\ year^{-1}$ ), f) Human Development Index ( $year^{-1}$ ), g) Nitrogen deposition ( $kg\ m^{-2}\ day^{-1}\ year^{-1}$ ), and h) Carbon Dioxide mixing ratio ( $kg\ m^{-2}\ day^{-1}\ year^{-1}$ ).

**Table A1.** Annual burnt area statistics for the different GFED4s fire regions (Giglio et al., 2013).

	GLOBAL	BONA	TENA	CEAM	NHSA	SHSA	EURO	MIDE	NHAF	SHAF	BOAS	CEAS	SEAS	EQAS	AUST
GFED4s															
Mean BA (Mha)	476.43	2.47	2.33	1.68	4.94	25.85	0.86	0.90	152.24	155.85	7.65	19.22	12.85	0.70	39.88
Trend (Mha year <sup>-1</sup> )	-6.77	0.05	0.05	-0.04	-0.05	-0.44	-0.03	0.02	-2.20	-0.54	-0.03	-0.37	0.18	-0.02	-1.09
Mean BA (Mha)	442.08	4.09	19.53	6.08	1.97	75.09	3.09	4.78	136.30	85.29	10.21	14.88	13.89	0.11	31.43
Trend (Mha year <sup>-1</sup> )	-2.24	-0.02	0.09	0.00	0.02	-0.13	0.01	-0.04	-1.26	-0.14	0.05	0.10	0.08	0.00	0.02
Bias (Mha)	-34.35	1.62	17.21	4.40	-2.97	49.24	2.23	3.88	-15.94	-70.56	2.56	-4.34	1.03	-0.59	-8.46
Relative bias (%)	-7.21	65.27	739.79	262.03	-60.16	190.48	258.82	432.09	-10.47	-45.27	33.48	-22.58	8.05	-84.81	-21.20
RMSE	47.28	2.10	17.38	4.52	3.07	49.85	2.27	3.92	20.23	71.17	4.26	7.16	1.91	0.89	21.60
RMSE <sub>UE</sub>	32.50	1.35	2.43	1.00	0.77	7.78	0.45	0.55	12.45	9.31	3.40	5.69	1.60	0.66	19.87
Correlation	0.753	0.002	0.816	0.548	0.583	0.479	0.153	-0.260	0.777	0.468	0.267	0.138	0.688	0.798	0.870
STD / STD <sub>GFED4s</sub>	0.52	0.23	4.41	0.84	0.67	0.77	0.68	0.81	0.64	0.43	0.21	0.20	0.50	0.10	0.18
RMSE / STD <sub>GFED4s</sub>	2.14	1.64	29.46	4.28	3.41	6.18	6.54	11.77	1.35	7.07	1.21	1.33	0.99	1.32	1.14
RMSE <sub>UE</sub> / STD <sub>GFED4s</sub>	1.47	1.05	4.13	0.95	0.86	0.96	1.28	1.65	0.83	0.92	0.97	1.06	0.83	0.98	1.05
Mean BA (Mha)	278.90	0.52	3.40	2.13	0.29	25.58	0.45	3.09	125.08	69.65	3.43	6.50	9.56	0.03	7.14
Trend (Mha year <sup>-1</sup> )	-7.58	-0.02	-0.07	-0.05	-0.01	-0.64	-0.01	-0.11	-2.71	-1.94	-0.09	-0.22	-0.19	0.00	-0.20
Bias (Mha)	-197.52	-1.95	1.07	0.45	-4.65	-0.27	-0.41	2.19	-27.16	-86.20	-4.22	-12.72	-3.30	-0.67	-32.74
Relative bias (%)	-41.46	-78.97	46.08	26.56	-94.14	-1.05	-48.14	244.36	-17.84	-55.31	-55.17	-66.19	-25.64	-95.88	-82.09
RMSE	198.99	2.37	1.34	1.03	4.73	7.87	0.53	2.35	29.19	87.11	5.44	13.80	4.23	0.97	38.14
RMSE <sub>UE</sub>	24.12	1.34	0.81	0.92	0.89	7.87	0.33	0.84	10.70	12.60	3.44	5.36	2.66	0.70	19.57
Correlation	0.842	-0.141	0.391	0.614	0.641	0.377	0.732	-0.248	0.863	0.390	0.231	0.370	-0.663	0.850	0.216
STD / STD <sub>GFED4s</sub>	0.42	0.04	1.04	0.34	0.09	0.28	0.15	0.63	0.68	0.48	0.09	0.10	0.40	0.03	0.06
RMSE / STD <sub>GFED4s</sub>	9.00	1.85	2.28	0.97	5.26	0.98	1.53	7.06	1.95	8.65	1.55	2.57	2.20	1.44	2.01
RMSE <sub>UE</sub> / STD <sub>GFED4s</sub>	1.09	1.04	1.37	0.88	0.98	0.98	0.96	2.53	0.71	1.25	0.98	1.00	1.38	1.04	1.03
JULES-INFERNO+HDI															

**Table A2.** JULES-INFERNO burnt area trends ( $Mha\ year^{-1}$ ) for the different GFED4s fire regions (Giglio et al., 2013) from the model sensitivity experiments. The standard error of the estimated trend, under the assumption of residual normality is shown in brackets. Values in bold represent trends that are significantly different from zero at the 99.95% confidence level.

	GFED4s	JULES-INFERNO								
		<i>control</i>	<i>1990 control</i>	<i>clim</i>	<i>tas</i>	<i>ppn</i>	<i>lu</i>	<i>Ndep</i>	<i>pop</i>	<i>CO2</i>
<b>GLOBAL</b>	<b>-6.77</b> (9.8e-01)	<b>-2.24</b> (5.1e-01)	-0.26 (5.3e-01)	-0.06 (5.5e-01)	0.42 (4.7e-01)	-0.92 (4.9e-01)	-1.01 (5.4e-01)	-0.27 (5.3e-01)	-1.45 (4.7e-01)	-0.32 (6.0e-01)
<b>BONA</b>	0.048 (5.2e-02)	-0.017 (1.3e-02)	0.002 (1.9e-03)	-0.023 (1.2e-02)	0.008 (1.5e-02)	-0.007 (7.7e-03)	0.003 (1.8e-03)	0.002 (1.8e-03)	0.005 (1.8e-03)	0.003 (1.8e-03)
<b>TENA</b>	0.05 (2.4e-02)	0.08 (1.2e-01)	0.01 (1.1e-02)	0.04 (1.1e-01)	0.08 (2.9e-02)	-0.05 (6.7e-02)	<b>0.05</b> (9.3e-03)	0.01 (1.2e-02)	-0.02 (1.1e-02)	0.05 (1.2e-02)
<b>CEAM</b>	-0.07 (4.3e-02)	0.000 (3.9e-02)	0.01 (9.1e-03)	0.03 (4.2e-02)	0.03 (1.4e-02)	0.02 (3.9e-02)	0.01 (8.6e-03)	0.01 (9.1e-03)	-0.01 (8.9e-03)	0.01 (9.2e-03)
<b>NHSA</b>	-0.05 (3.7e-02)	0.02 (2.6e-02)	0.001 (7.5e-04)	0.03 (2.6e-02)	0.01 (6.0e-03)	0.02 (1.8e-02)	0.002 (9.4e-04)	0.001 (7.5e-04)	-0.002 (7.9e-04)	-0.005 (1.5e-03)
<b>SHSA</b>	-0.41 (3.3e-01)	-0.12 (2.6e-01)	0.04 (8.3e-02)	0.14 (2.8e-01)	0.27 (7.3e-02)	-0.17 (2.2e-01)	-0.17 (8.6e-02)	0.04 (8.3e-02)	-0.005 (8.2e-02)	-0.01 (9.4e-02)
<b>EURO</b>	-0.03 (1.4e-02)	0.01 (1.1e-02)	0.001 (3.5e-03)	-0.001 (1.0e-02)	0.01 (3.9e-03)	-0.01 (7.4e-03)	<b>0.01</b> (2.0e-03)	0.0005 (3.4e-03)	-0.01 (3.5e-03)	0.003 (3.2e-03)
<b>MIDE</b>	0.02 (1.4e-02)	-0.04 (1.2e-02)	0.001 (7.8e-03)	-0.02 (1.3e-02)	0.01 (9.9e-03)	-0.04 (1.2e-02)	0.001 (7.8e-03)	-0.003 (9.4e-03)	<b>-0.04</b> (6.9e-03)	0.01 (7.6e-03)
<b>NHAF</b>	-2.24 (6.1e-01)	-1.35 (5.1e-01)	0.04 (3.1e-01)	0.15 (5.2e-01)	0.14 (3.2e-01)	-0.10 (5.3e-01)	-0.35 (3.3e-01)	0.04 (3.1e-01)	-0.55 (2.7e-01)	0.06 (3.2e-01)
<b>SHAF</b>	-0.53 (4.1e-01)	-0.15 (1.9e-01)	0.17 (1.4e-01)	0.27 (1.9e-01)	0.15 (1.4e-01)	0.15 (1.4e-01)	0.01 (1.4e-01)	0.17 (1.4e-01)	-0.18 (1.4e-01)	0.04 (1.6e-01)
<b>BOAS</b>	-0.07 (1.4e-01)	0.05 (3.1e-02)	0.01 (4.2e-03)	0.04 (2.9e-02)	0.06 (2.1e-02)	0.03 (1.5e-02)	0.02 (3.9e-03)	0.01 (4.0e-03)	-0.01 (3.9e-03)	0.01 (4.1e-03)
<b>CEAS</b>	-0.35 (2.2e-01)	0.10 (4.6e-02)	0.01 (7.3e-03)	0.08 (5.0e-02)	0.05 (2.4e-02)	0.03 (2.6e-02)	0.02 (8.0e-03)	0.01 (6.7e-03)	0.01 (7.5e-03)	0.03 (9.2e-03)
<b>SEAS</b>	0.17 (7.9e-02)	0.07 (4.4e-02)	0.02 (8.6e-03)	0.06 (4.3e-02)	0.03 (2.4e-02)	0.05 (3.3e-02)	0.0004 (7.6e-03)	0.02 (7.9e-03)	<b>0.04</b> (8.4e-03)	0.02 (9.0e-03)
<b>EQAS</b>	-0.04 (2.8e-02)	-0.0027 (3.0e-03)	0.0004 (2.2e-04)	-0.0020 (3.3e-03)	0.0003 (3.3e-04)	-0.0017 (2.5e-03)	-0.0001 (2.2e-04)	0.0004 (2.2e-04)	-0.0002 (2.0e-04)	0.0003 (2.2e-04)
<b>AUST</b>	-1.02 (7.8e-01)	0.01 (1.4e-01)	0.07 (5.6e-02)	-0.05 (1.5e-01)	0.12 (5.9e-02)	-0.12 (1.3e-01)	0.07 (5.6e-02)	0.06 (5.6e-02)	0.07 (5.6e-02)	0.11 (5.8e-02)

**Table A3.** JULES-INFERNO+HDI burnt area trends ( $Mha\ year^{-1}$ ) for the different GFED4s fire regions (Giglio et al., 2013) from the model sensitivity experiments. The standard error of the estimated trend, under the assumption of residual normality is shown in brackets. Values in bold represent trends that are significantly different from zero at the 99.95 % confidence level.

	GFED4s	JULES-INFERNO+HDI									
		<i>control</i>	<i>1990 control</i>	<i>clim</i>	<i>tas</i>	<i>ppn</i>	<i>lu</i>	<i>Ndep</i>	<i>pop</i>	<i>CO2</i>	<i>HDI</i>
<b>GLOBAL</b>	<b>-6.77</b> (9.8e-01)	<b>0.15</b> (2.2e-02)	<b>-7.58</b> (4.2e-01)	0.24 (5.5e-01)	0.58 (2.1e-01)	-0.60 (5.5e-01)	<b>-0.97</b> (2.0e-02)	<b>0.16</b> (2.3e-02)	<b>-0.91</b> (1.9e-02)	0.02 (2.3e-02)	<b>-4.27</b> (9.8e-02)
<b>BONA</b>	0.048 (5.2e-02)	-0.0002 (8.2e-05)	<b>-0.023</b> (2.1e-03)	-0.006 (2.8e-03)	0.002 (2.8e-03)	-0.003 (1.9e-03)	-0.0002 (8.2e-05)	-0.0002 (8.3e-05)	-0.0003 (8.0e-05)	-0.0001 (8.1e-05)	<b>-0.021</b> (6.6e-04)
<b>TENA</b>	0.05 (2.4e-02)	0.00 (7.1e-04)	-0.07 (2.8e-02)	0.001 (3.6e-02)	0.02 (8.3e-03)	-0.02 (2.2e-02)	<b>0.01</b> (8.4e-04)	0.000 (8.3e-04)	<b>-0.01</b> (7.9e-04)	<b>0.004</b> (8.0e-04)	<b>-0.05</b> (1.7e-03)
<b>CEAM</b>	-0.07 (4.3e-02)	<b>-0.01</b> (1.5e-03)	-0.04 (1.6e-02)	0.02 (2.3e-02)	0.01 (3.8e-03)	0.01 (2.3e-02)	-0.01 (1.6e-03)	<b>-0.01</b> (1.5e-03)	<b>-0.02</b> (1.4e-03)	-0.01 (1.7e-03)	<b>-0.05</b> (1.5e-03)
<b>NHSA</b>	-0.05 (3.7e-02)	0.000 (1.2e-04)	-0.01 (3.7e-03)	0.01 (5.8e-03)	0.003 (1.5e-03)	0.003 (3.9e-03)	<b>-0.001</b> (1.0e-04)	-0.0005 (1.2e-04)	<b>-0.001</b> (1.3e-04)	<b>-0.004</b> (1.5e-04)	<b>-0.01</b> (4.7e-04)
<b>SHSA</b>	-0.41 (3.3e-01)	0.05 (2.1e-02)	<b>-0.62</b> (9.7e-02)	0.11 (1.4e-01)	<b>0.14</b> (3.1e-02)	-0.09 (1.1e-01)	-0.06 (2.4e-02)	0.05 (2.1e-02)	0.02 (2.1e-02)	-0.002 (2.3e-02)	<b>-0.34</b> (1.9e-02)
<b>EURO</b>	-0.03 (1.4e-02)	-0.0002 (1.2e-04)	<b>-0.01</b> (2.4e-03)	-0.0001 (3.1e-03)	<b>0.004</b> (9.2e-04)	-0.003 (2.1e-03)	<b>0.004</b> (1.3e-04)	-0.0002 (1.2e-04)	<b>-0.002</b> (1.5e-04)	<b>0.001</b> (1.3e-04)	<b>-0.01</b> (4.4e-04)
<b>MIDE</b>	0.02 (1.4e-02)	<b>0.02</b> (3.0e-03)	<b>-0.11</b> (8.9e-03)	-0.004 (1.5e-02)	<b>0.03</b> (5.7e-03)	-0.02 (1.5e-02)	<b>0.02</b> (2.6e-03)	<b>0.02</b> (4.4e-03)	<b>-0.03</b> (3.0e-03)	<b>0.04</b> (2.5e-03)	<b>-0.09</b> (4.8e-03)
<b>NHAF</b>	-2.24 (6.1e-01)	0.14 (7.1e-02)	<b>-2.78</b> (5.5e-01)	0.50 (6.3e-01)	0.33 (1.2e-01)	0.12 (6.0e-01)	<b>-0.57</b> (6.6e-02)	0.14 (7.2e-02)	<b>-0.31</b> (7.3e-02)	0.24 (7.6e-02)	<b>-0.73</b> (9.0e-02)
<b>SHAF</b>	-0.53 (4.1e-01)	0.29 (1.3e-01)	<b>-1.92</b> (2.1e-01)	0.28 (2.2e-01)	0.24 (1.5e-01)	0.05 (1.5e-01)	0.03 (1.3e-01)	0.30 (1.3e-01)	-0.09 (1.3e-01)	0.07 (1.3e-01)	<b>-1.48</b> (1.7e-01)
<b>BOAS</b>	-0.07 (1.4e-01)	0.001 (9.0e-04)	<b>-0.10</b> (1.3e-02)	0.02 (1.2e-02)	0.02 (6.2e-03)	0.02 (6.8e-03)	<b>0.005</b> (8.8e-04)	0.002 (9.3e-04)	-0.002 (8.7e-04)	0.003 (9.1e-04)	<b>-0.12</b> (5.0e-03)
<b>CEAS</b>	-0.35 (2.2e-01)	0.01 (5.0e-03)	<b>-0.23</b> (2.3e-02)	0.04 (3.1e-02)	0.04 (1.2e-02)	0.02 (1.7e-02)	<b>0.02</b> (4.5e-03)	0.02 (4.4e-03)	0.01 (5.0e-03)	<b>0.03</b> (4.9e-03)	<b>-0.23</b> (8.1e-03)
<b>SEAS</b>	0.17 (7.9e-02)	0.02 (7.7e-03)	<b>-0.19</b> (3.5e-02)	0.08 (4.5e-02)	0.04 (2.5e-02)	0.06 (3.7e-02)	0.004 (7.4e-03)	0.02 (7.0e-03)	<b>0.04</b> (7.6e-03)	0.02 (7.6e-03)	<b>-0.19</b> (7.7e-03)
<b>EQAS</b>	-0.04 (2.8e-02)	0.0003 (1.1e-04)	-0.0014 (8.3e-04)	-0.0005 (1.3e-03)	0.0003 (1.3e-04)	-0.0005 (9.9e-04)	-0.0001 (1.1e-04)	0.0003 (1.1e-04)	0.0001 (9.5e-05)	0.0002 (1.1e-04)	<b>-0.001</b> (1.0e-04)
<b>AUST</b>	-1.02 (7.8e-01)	0.03 (1.9e-02)	-0.19 (5.3e-02)	0.01 (7.2e-02)	0.06 (2.5e-02)	-0.01 (6.5e-02)	0.03 (1.9e-02)	0.03 (1.9e-02)	0.03 (1.9e-02)	0.04 (1.9e-02)	<b>-0.17</b> (1.6e-02)

1045 . Both the model code and the files for running it are available from the Met Office Science Repository Service: <https://code.metoffice.gov.uk/> (last access: 26 July 2023). Registration is required, and code is freely available subject to completion of a software license.

Details of the simulations performed: JULES simulations are compiled and run in suites developed using the Rose suite engine (MetOffice, 2022) and scheduled using the cylc workflow engine (Oliver et al., 2019). Both Rose and cylc are available under v3 of the GNU General Public License (GPL). In this framework, the suite contains the information required to extract and build the code as well as configure and  
1050 run the simulations. Each suite is labelled with a unique identifier and is held in the same revision-controlled repository service in which we hold and develop the model code. This means that these suites are available to any licensed of JULES under the following suite IDs:

- JULES-INFERNO: u-by849
- JULES-INFERNO+HDI: u-by851

For JULES-INFERNO sensitivity experiments:

- 1055 – 1990 control: u-co594
- clim: u-cs067
- tas: u-cs068
- ppn: u-cs069
- lu: u-cr440

- 1060 – Ndep: u-cr441
- pop: u-cr442
- CO<sub>2</sub>: u-cr443

For JULES-INFERNO+HDI sensitivity experiments:

- 1990 control: u-ct759
- 1065 – clim: u-cs070
- tas: u-cs071
- ppn: u-cs072
- lu: u-cr447
- Ndep: u-cr448
- 1070 – pop: u-cr449
- CO<sub>2</sub>: u-cr450
- HDI: u-cn957

. JCMT led the writing of the paper and model development. All co-authors contributed to the simulation design, writing sections, performing evaluation and reviewing drafts of the paper.

1075 . At least one of the (co-)authors is a member of the editorial board of Earth System Dynamics.

. We would especially like to thank those who have contributed to the development of INFERNO, with a special thanks to Stéphane Mangeon for taking the first steps to develop INFERNO and the observational community, who have developed numerous datasets used in this paper to help evaluate the model.

1080 This research and JCMT, CB, GAF, FMOC, RAB were supported by the Met Office Hadley Centre Climate Programme funded by DSIT. JCMT, GAF, and FMOC were also supported by the Horizon 2020 Framework Programme (CRESCENDO, grant no. 779366) and the Earth System Models for the Future (ESM2025, grant no. 101003536). CB was funded by the Met Office Climate Science for Service Partnership (CSSP) Brazil project which is supported by the Department for Science, Innovation & Technology (DSIT). DIK was supported by the Natural Environment Research Council as part of the LTSM2 TerraFIRMA project. AV was funded via the Leverhulme Centre for Wildfires, Environment and Society through the Leverhulme Trust, grant no. RC-2018-023.

- Abatzoglou, J. T. and Williams, A. P.: Impact of anthropogenic climate change on wildfire across western US forests, *Proceedings of the National Academy of Sciences*, 113, 11 770–11 775, 2016.
- Abatzoglou, J. T., Williams, A. P., Boschetti, L., Zubkova, M., and Kolden, C. A.: Global patterns of interannual climate–fire relationships, *Global change biology*, 24, 5164–5175, 2018.
- 1090 Andela, N. and Van Der Werf, G. R.: Recent trends in African fires driven by cropland expansion and El Nino to La Nina transition, *Nature Climate Change*, 4, 791–795, 2014.
- Andela, N., Morton, D. C., Giglio, L., Chen, Y., van der Werf, G. R., Kasibhatla, P. S., DeFries, R. S., Collatz, G., Hantson, S., Kloster, S., et al.: A human-driven decline in global burned area, *Science*, 356, 1356–1362, 2017.
- Andela, N., Morton, D. C., Giglio, L., Paugam, R., Chen, Y., Hantson, S., Van Der Werf, G. R., and Randerson, J. T.: The Global Fire Atlas  
1095 of individual fire size, duration, speed and direction, *Earth System Science Data*, 11, 529–552, 2019.
- Aragão, L. E., Anderson, L. O., Fonseca, M. G., Rosan, T. M., Vedovato, L. B., Wagner, F. H., Silva, C. V., Silva Junior, C. H., Arai, E., Aguiar, A. P., et al.: 21st Century drought-related fires counteract the decline of Amazon deforestation carbon emissions, *Nature communications*, 9, 536, 2018.
- Archibald, S., Nickless, A., Govender, N., Scholes, R. J., and Lehsten, V.: Climate and the inter-annual variability of fire in southern Africa:  
1100 a meta-analysis using long-term field data and satellite-derived burnt area data, *Global Ecology and Biogeography*, 19, 794–809, 2010.
- Benjamini, Y. and Yekutieli, D.: The control of the false discovery rate in multiple testing under dependency, *Annals of statistics*, pp. 1165–1188, 2001.
- Best, M. J., Pryor, M., Clark, D. B., Rooney, G. G., Essery, R. L. H., Ménard, C. B., Edwards, J. M., Hendry, M. A., Porson, A., Gedney, N., Mercado, L. M., Sitch, S., Blyth, E., Boucher, O., Cox, P. M., Grimmond, C. S. B., and Harding, R. J.: The Joint UK Land  
1105 Environment Simulator (JULES), model description – Part 1: Energy and water fluxes, *Geoscientific Model Development*, 4, 677–699, <https://doi.org/10.5194/gmd-4-677-2011>, 2011.
- Bhanojirao, V.: Human development report 1990: review and assessment, *World Development*, 19, 1451–1460, 1991.
- Blackford, K. R., Kasoar, M., Burton, C., Burke, E., Prentice, I. C., and Voulgarakis, A.: INFERNO-peat v1. 0.0: a representation of northern high-latitude peat fires in the JULES-INFERNO global fire model, *Geoscientific Model Development*, 17, 3063–3079, 2024.
- 1110 Bowman, D. M., Kolden, C. A., Abatzoglou, J. T., Johnston, F. H., van der Werf, G. R., and Flannigan, M.: Vegetation fires in the Anthropocene, *Nature Reviews Earth & Environment*, 1, 500–515, 2020.
- Burton, C., Betts, R., Cardoso, M., Feldpausch, T. R., Harper, A., Jones, C. D., Kelley, D. I., Robertson, E., and Wiltshire, A.: Representation of fire, land-use change and vegetation dynamics in the Joint UK Land Environment Simulator vn4.9 (JULES), *Geoscientific Model Development*, 12, 179–193, <https://doi.org/10.5194/gmd-12-179-2019>, 2019.
- 1115 Burton, C., Betts, R. A., Jones, C. D., Feldpausch, T. R., Cardoso, M., and Anderson, L. O.: El Niño Driven Changes in Global Fire 2015/16, *Frontiers in Earth Science*, 8, 199, <https://doi.org/10.3389/feart.2020.00199>, 2020.
- Burton, C. A., Kelley, D. I., Burke, E., Mathison, C., Jones, C. D., Betts, R. A., Robertson, E., Teixeira, J. C., Cardoso, M., and Anderson, L. O.: Fire weakens land carbon sinks before 1.5° C, *Nature Geoscience*, 17, 1108–1114, 2024.
- Carreiras, M., Ferreira, A. J. D., Valente, S., Fleskens, L., Gonzales-Pelayo, Ó., Rubio, J. L., Stoof, C. R., Coelho, C. O. A., Ferreira, C. S. S.,  
1120 and Ritsema, C. J.: Comparative analysis of policies to deal with wildfire risk, *Land Degradation & Development*, 25, 92–103, 2014.
- Cecil, D.: LIS/OTD 0.5 Degree High Resolution Monthly Climatology (HRMC), <https://doi.org/10.3389/feart.2020.00199>, 2006.

- Chergui, B., Fahd, S., Santos, X., and Pausas, J. G.: Socioeconomic factors drive fire-regime variability in the Mediterranean Basin, *Ecosystems*, 21, 619–628, 2018.
- Christian, H. J., Blakeslee, R. J., Boccippio, D. J., Boeck, W. L., Buechler, D. E., Driscoll, K. T., Goodman, S. J., Hall, J. M., Koshak, W. J., Mach, D. M., et al.: Global frequency and distribution of lightning as observed from space by the Optical Transient Detector, *Journal of Geophysical Research: Atmospheres*, 108, ACL–4, 2003.
- 1125 Chuvieco, E., Pettinari, M. L., Koutsias, N., Forkel, M., Hantson, S., and Turco, M.: Human and climate drivers of global biomass burning variability, *Science of the Total Environment*, 779, 146–361, 2021.
- Clark, D. B., Mercado, L. M., Sitch, S., Jones, C. D., Gedney, N., Best, M. J., Pryor, M., Rooney, G. G., Essery, R. L. H., Blyth, E., Boucher, O., Harding, R. J., Huntingford, C., and Cox, P. M.: The Joint UK Land Environment Simulator (JULES), model description – Part 2: Carbon fluxes and vegetation dynamics, *Geoscientific Model Development*, 4, 701–722, <https://doi.org/10.5194/gmd-4-701-2011>, 2011.
- 1130 Cox, P.: Description of the "TRIFFID" Dynamic Global Vegetation Mode, 2001.
- Cox, P., Betts, R., Jones, C., Spall, S., and Totterdell, I.: Acceleration of global warming due to carbon-cycle feedbacks in a coupled climate model, *Nature*, 408, 184–187, 2000.
- 1135 Curt, T. and Frejaville, T.: Wildfire policy in Mediterranean France: how far is it efficient and sustainable?, *Risk analysis*, 38, 472–488, 2018.
- Duane, A., Aquilué, N., Canelles, Q., Morán-Ordoñez, A., De Cáceres, M., and Brotons, L.: Adapting prescribed burns to future climate change in Mediterranean landscapes, *Science of the Total Environment*, 677, 68–83, 2019.
- Eyring, V., Bony, S., Meehl, G. A., Senior, C. A., Stevens, B., Stouffer, R. J., and Taylor, K. E.: Overview of the Coupled Model Intercomparison Project Phase 6 (CMIP6) experimental design and organization, *Geoscientific Model Development*, 9, 1937–1958, 2016.
- 1140 Field, R., Spessa, A., Aziz, N., Camia, A., Cantin, A., Carr, R., De Groot, W., Dowdy, A., Flannigan, M., Manomaiphiboon, K., et al.: Development of a global fire weather database, *Natural Hazards and Earth System Sciences*, 15, 1407–1423, 2015.
- Ford, A. E., Harrison, S. P., Kountouris, Y., Millington, J. D., Mistry, J., Perkins, O., Rabin, S. S., Rein, G., Schreckenber, K., Smith, C., et al.: Modelling human–fire interactions: combining alternative perspectives and approaches, *Frontiers in Environmental Science*, p. 418, 2021.
- 1145 Forkel, M., Andela, N., Harrison, S. P., Lasslop, G., Van Marle, M., Chuvieco, E., Dorigo, W., Forrest, M., Hantson, S., Heil, A., et al.: Emergent relationships with respect to burned area in global satellite observations and fire-enabled vegetation models, *Biogeosciences*, 16, 57–76, 2019.
- Giglio, L., Randerson, J. T., and Van Der Werf, G. R.: Analysis of daily, monthly, and annual burned area using the fourth-generation global fire emissions database (GFED4), *Journal of Geophysical Research: Biogeosciences*, 118, 317–328, 2013.
- 1150 Gillson, L., Whitlock, C., and Humphrey, G.: Resilience and fire management in the Anthropocene, *Ecology and Society*, 24, 2019.
- Goldewijk, K. K., Dekker, S. C., and van Zanden, J. L.: Per-capita estimations of long-term historical land use and the consequences for global change research, *Journal of Land Use Science*, 12, 313–337, <https://doi.org/10.1080/1747423X.2017.1354938>, 2017.
- Goss, M., Swain, D. L., Abatzoglou, J. T., Sarhadi, A., Kolden, C. A., Williams, A. P., and Diffenbaugh, N. S.: Climate change is increasing the likelihood of extreme autumn wildfire conditions across California, *Environmental Research Letters*, 15, 094–016, 2020.
- 1155 Haas, O., Prentice, I. C., and Harrison, S. P.: Global environmental controls on wildfire burnt area, size, and intensity, *Environmental Research Letters*, 17, 065–004, 2022.
- Haas, O., Prentice, I., and Harrison, S.: Global wildfires on a changing planet - in review, 2024.
- Harris, I., Jones, P. D., Osborn, T. J., and Lister, D. H.: Updated high-resolution grids of monthly climatic observations—the CRU TS3. 10 Dataset, *International journal of climatology*, 34, 623–642, 2014.

- 1160 Hickel, J.: The sustainable development index: Measuring the ecological efficiency of human development in the anthropocene, *Ecological economics*, 167, 106331, 2020.
- Jacobson, M., Smith, H., Huber-Stearns, H. R., Davis, E. J., Cheng, A. S., and Deak, A.: Comparing social constructions of wildfire risk across media, government, and participatory discourse in a Colorado fireshed, *Journal of Risk Research*, 25, 697–714, 2022.
- Jones, M. W., Abatzoglou, J. T., Veraverbeke, S., Andela, N., Lasslop, G., Forkel, M., Smith, A. J., Burton, C., Betts, R. A., van der Werf, G. R., et al.: Global and regional trends and drivers of fire under climate change, *Reviews of Geophysics*, p. e2020RG000726, 2022.
- 1165 Jones, M. W., Kelley, D. I., Burton, C. A., Di Giuseppe, F., Barbosa, M. L. F., Brambleby, E., Hartley, A. J., Lombardi, A., Mataveli, G., McNorton, J. R., et al.: State of wildfires 2023–2024, *Earth System Science Data*, 16, 3601–3685, 2024.
- Kasischke, E. S. and Turetsky, M. R.: Recent changes in the fire regime across the North American boreal region—Spatial and temporal patterns of burning across Canada and Alaska, *Geophysical research letters*, 33, 2006.
- 1170 Kelley, D. I., Bistinas, I., Whitley, R., Burton, C., Marthews, T. R., and Dong, N.: How contemporary bioclimatic and human controls change global fire regimes, *Nature Climate Change*, 9, 690–696, 2019.
- Kirillina, K., Shvetsov, E. G., Protopopova, V. V., Thiesmeyer, L., and Yan, W.: Consideration of anthropogenic factors in boreal forest fire regime changes during rapid socio-economic development: case study of forestry districts with increasing burnt area in the Sakha Republic, Russia, *Environmental Research Letters*, 15, 035009, 2020.
- 1175 Klauenberg, K., Wübbeler, G., Mickan, B., Harris, P., and Elster, C.: A tutorial on Bayesian normal linear regression, *Metrologia*, 52, 878, 2015.
- Klein Goldewijk, K., Beusen, A., Doelman, J., and Stehfest, E.: Anthropogenic land use estimates for the Holocene – HYDE 3.2, *Earth System Science Data*, 9, 927–953, <https://doi.org/10.5194/essd-9-927-2017>, 2017.
- Kummu, M., Taka, M., and Guillaume, J. H.: Gridded global datasets for gross domestic product and Human Development Index over 1990–2015, *Scientific data*, 5, 180004, 2018.
- 1180 Lasslop, G., Thonicke, K., and Kloster, S.: SPITFIRE within the MPI Earth system model: Model development and evaluation, *Journal of Advances in Modeling Earth Systems*, 6, 740–755, 2014.
- Li, F., Levis, S., and Ward, D.: Quantifying the role of fire in the Earth system—Part 1: Improved global fire modeling in the Community Earth System Model (CESM1), *Biogeosciences*, 10, 2293–2314, 2013.
- 1185 Li, F., Song, X., Harrison, S. P., Marlon, J. R., Lin, Z., Leung, L. R., Schwinger, J., Marécal, V., Wang, S., Ward, D. S., et al.: Evaluation of global fire simulations in CMIP6 Earth system models, *Geoscientific Model Development Discussions*, 2024, 1–37, 2024.
- Mangeon, S., Voulgarakis, A., Gilham, R., Harper, A., Sitch, S., and Folberth, G.: INFERNO: a fire and emissions scheme for the UK Met Office’s Unified Model, *Geoscientific Model Development*, 9, 2685–2700, 2016.
- Marlon, J. R., Bartlein, P. J., Carcaillet, C., Gavin, D. G., Harrison, S. P., Higuera, P. E., Joos, F., Power, M., and Prentice, I.: Climate and 1190 human influences on global biomass burning over the past two millennia, *Nature Geoscience*, 1, 697–702, 2008.
- Mathison, C., Burke, E., Hartley, A. J., Kelley, D. I., Burton, C., Robertson, E., Gedney, N., Williams, K., Wiltshire, A., Ellis, R. J., et al.: Description and Evaluation of the JULES-ES setup for ISIMIP2b, *EGUsphere*, 2022, 1–24, 2022.
- MetOffice: Rose suite engine, <https://metomi.github.io/rose/doc/html/index.html>, 2022.
- Miranda-Lescano, R., Muinel-Gallo, L., and Roca-Sagalés, O.: Human development and decentralization: The importance of public health 1195 expenditure, *Annals of Public and Cooperative Economics*, 94, 191–219, 2023.
- Mourão, P. R. and Martinho, V. D.: The choices of the fire—Debating socioeconomic determinants of the fires observed at Portuguese municipalities, *Forest Policy and Economics*, 43, 29–40, 2014.

- Nepstad, D., McGrath, D., Stickler, C., Alencar, A., Azevedo, A., Swette, B., Bezerra, T., DiGiano, M., Shimada, J., Seroa da Motta, R., et al.: Slowing Amazon deforestation through public policy and interventions in beef and soy supply chains, *science*, 344, 1118–1123, 2014.
- 1200
- Nikolakis, W. and Roberts, E.: Wildfire governance in a changing world: Insights for policy learning and policy transfer, *Risk, Hazards & Crisis in Public Policy*, 13, 144–164, 2022.
- Oliver, H., Shin, M., Matthews, D., Sanders, O., Bartholomew, S., Clark, A., Fitzpatrick, B., van Haren, R., Hut, R., and Drost, N.: Workflow automation for cycling systems, *Computing in Science & Engineering*, 21, 7–21, 2019.
- 1205
- Pandey, P., Huidobro, G., Lopes, L. F., Ganteaume, A., Ascoli, D., Colaco, C., Xanthopoulos, G., Giannaros, T. M., Gazzard, R., Boustras, G., et al.: A global outlook on increasing wildfire risk: Current policy situation and future pathways, *Trees, Forests and People*, 14, 100431, 2023.
- Paveglio, T. B., Carroll, M. S., Stasiewicz, A. M., Williams, D. R., and Becker, D. R.: Incorporating social diversity into wildfire management: Proposing “pathways” for fire adaptation, *Forest Science*, 64, 515–532, 2018.
- 1210
- Pechony, O. and Shindell, D.: Fire parameterization on a global scale, *Journal of Geophysical Research: Atmospheres*, 114, 2009.
- Perkins, O., Kasoar, M., Voulgarakis, A., Smith, C., Mistry, J., and Millington, J. D.: A global behavioural model of human fire use and management: WHAM! v1. 0, *Geoscientific Model Development*, 17, 3993–4016, 2024.
- Pivello, V. R., Vieira, I., Christianini, A. V., Ribeiro, D. B., da Silva Menezes, L., Berlinck, C. N., Melo, F. P., Marengo, J. A., Tornquist, C. G., Tomas, W. M., et al.: Understanding Brazil’s catastrophic fires: Causes, consequences and policy needed to prevent future tragedies, *Perspectives in Ecology and Conservation*, 19, 233–255, 2021.
- 1215
- Prestemon, J. P., Butry, D. T., Abt, K. L., and Sutphen, R.: Net benefits of wildfire prevention education efforts, *Forest Science*, 56, 181–192, 2010.
- Rabin, S. S., Melton, J. R., Lasslop, G., Bachelet, D., Forrest, M., Hantson, S., Kaplan, J. O., Li, F., Mangeon, S., Ward, D. S., et al.: The Fire Modeling Intercomparison Project (FireMIP), phase 1: experimental and analytical protocols with detailed model descriptions, *Geoscientific Model Development*, 10, 1175–1197, 2017.
- 1220
- Ramdas, A., García Trillos, N., and Cuturi, M.: On wasserstein two-sample testing and related families of nonparametric tests, *Entropy*, 19, 47, 2017.
- Randerson, J., Chen, Y., Van Der Werf, G., Rogers, B., and Morton, D.: Global burned area and biomass burning emissions from small fires, *Journal of Geophysical Research: Biogeosciences*, 117, 2012.
- 1225
- Rideout, D. B., Wei, Y., Kirsch, A., and Kernohan, N.: STARFire: Strategic budgeting and planning for wildland fire management, *Park Science*, 32, 34–41, 2017.
- Riley, K. L., Williams, A. P., Urbanski, S. P., Calkin, D. E., Short, K. C., and O’Connor, C. D.: Will landscape fire increase in the future? A systems approach to climate, fire, fuel, and human drivers, *Current Pollution Reports*, 5, 9–24, 2019.
- Rizzo, L. V. and Rizzo, M. C. F.: Wildfire smoke and health impacts: a narrative review, *Jornal de Pediatria*, 2024.
- 1230
- Roy, A., Dutta, T., Li, Y., and Dong, X.: Human development at the cost of the environment?—an application of planetary pressures—adjusted human development index in the lens of planetary boundaries, *Environmental Science and Pollution Research*, 30, 32 383–32 405, 2023.
- Sellar, A. A., Jones, C. G., Mulcahy, J. P., Tang, Y., Yool, A., Wiltshire, A., O’Connor, F. M., Stringer, M., Hill, R., Palmieri, J., Woodward, S., de Mora, L., Kuhlbrodt, T., Rumbold, S. T., Kelley, D. I., Ellis, R., Johnson, C. E., Walton, J., Abraham, N. L., Andrews, M. B., Andrews, T., Archibald, A. T., Berthou, S., Burke, E., Blockley, E., Carslaw, K., Dalvi, M., Edwards, J., Folberth, G. A., Gedney, N., Griffiths, P. T., Harper, A. B., Hendry, M. A., Hewitt, A. J., Johnson, B., Jones, A., Jones, C. D., Keeble, J., Liddicoat, S., Morgenstern,
- 1235

- O., Parker, R. J., Predoi, V., Robertson, E., Siahhaan, A., Smith, R. S., Swaminathan, R., Woodhouse, M. T., Zeng, G., and Zerroukat, M.: UKESM1: Description and Evaluation of the U.K. Earth System Model, *Journal of Advances in Modeling Earth Systems*, 11, 4513–4558, <https://doi.org/https://doi.org/10.1029/2019MS001739>, 2019a.
- 1240 Sellar, A. A., Jones, C. G., Mulcahy, J. P., Tang, Y., Yool, A., Wiltshire, A., O’connor, F. M., Stringer, M., Hill, R., Palmieri, J., et al.: UKESM1: Description and evaluation of the UK Earth System Model, *Journal of Advances in Modeling Earth Systems*, 11, 4513–4558, 2019b.
- Silva Junior, C. H., Pessôa, A. C., Carvalho, N. S., Reis, J. B., Anderson, L. O., and Aragão, L. E.: The Brazilian Amazon deforestation rate in 2020 is the greatest of the decade, *Nature Ecology & Evolution*, 5, 144–145, 2021.
- 1245 Stocks, B., Mason, J., Todd, J., Bosch, E., Wotton, B., Amiro, B., Flannigan, M., Hirsch, K., Logan, K., Martell, D., et al.: Large forest fires in Canada, 1959–1997, *Journal of Geophysical Research: Atmospheres*, 107, FFR–5, 2002.
- Sullivan, A., Kurvits, T., and E., B.: Spreading like Wildfire – The Rising Threat of Extraordinary Landscape Fires., United Nations Environment Programme (UNEP), 2022.
- Teckentrup, L., Harrison, S. P., Hantson, S., Heil, A., Melton, J. R., Forrest, M., Li, F., Yue, C., Arneeth, A., Hickler, T., et al.: Response of simulated burned area to historical changes in environmental and anthropogenic factors: a comparison of seven fire models, *Biogeosciences*, 16, 3883–3910, 2019.
- 1250 Teixeira, J. C., Folberth, G. A., O’Connor, F. M., Unger, N., and Voulgarakis, A.: Coupling interactive fire with atmospheric composition and climate in the UK Earth System Model, *Geoscientific Model Development*, 14, 6515–6539, 2021.
- Türe, C.: A methodology to analyse the relations of ecological footprint corresponding with human development index: eco-sustainable human development index, *International Journal of Sustainable Development & World Ecology*, 20, 9–19, 2013.
- 1255 Urbieto, I. R., Franquesa, M., Viedma, O., and Moreno, J. M.: Fire activity and burned forest lands decreased during the last three decades in Spain, *Annals of Forest Science*, 76, 1–13, 2019.
- Veraverbeke, S., Rogers, B. M., Goulden, M. L., Jandt, R. R., Miller, C. E., Wiggins, E. B., and Randerson, J. T.: Lightning as a major driver of recent large fire years in North American boreal forests, *Nature Climate Change*, 7, 529–534, 2017.
- Verjans, V., Franzke, C. L., Lee, S.-S., Kim, I.-W., Tilmes, S., Lawrence, D. M., Vitt, F., and Li, F.: Quantifying CO2 forcing effects on lightning, wildfires, and climate interactions, *Science Advances*, 11, eadt5088, 2025.
- 1260 Viovy, N.: CRUNCEP version 7-atmospheric forcing data for the community land model, Research Data Archive at the National Center for Atmospheric Research, Computational and Information Systems Laboratory, 10, 2018.
- Vitolo, C., Di Giuseppe, F., Barnard, C., Coughlan, R., San-Miguel-Ayanz, J., Libertá, G., and Krzeminski, B.: ERA5-based global meteorological wildfire danger maps, *Scientific data*, 7, 216, 2020.
- 1265 Williams, A. P., Abatzoglou, J. T., Gershunov, A., Guzman-Morales, J., Bishop, D. A., Balch, J. K., and Lettenmaier, D. P.: Observed impacts of anthropogenic climate change on wildfire in California, *Earth’s Future*, 7, 892–910, 2019.
- Williams, K., Copsey, D., Blockley, E., Bodas-Salcedo, A., Calvert, D., Comer, R., Davis, P., Graham, T., Hewitt, H., Hill, R., et al.: The Met Office global coupled model 3.0 and 3.1 (GC3. 0 and GC3. 1) configurations, *Journal of Advances in Modeling Earth Systems*, 10, 357–380, 2018.
- 1270 Yue, C., Ciais, P., Cadule, P., Thonicke, K., Archibald, S., Poulter, B., Hao, W., Hantson, S., Mouillot, F., Friedlingstein, P., et al.: Modelling the role of fires in the terrestrial carbon balance by incorporating SPITFIRE into the global vegetation model ORCHIDEE–Part 1: simulating historical global burned area and fire regimes, *Geoscientific Model Development*, 7, 2747–2767, 2014.

- Zou, Y., Wang, Y., Ke, Z., Tian, H., Yang, J., and Liu, Y.: Development of a REgion-specific ecosystem feedback fire (RESFire) model in the Community Earth System Model, *Journal of Advances in Modeling Earth Systems*, 11, 417–445, 2019.
- 1275 Zubkova, M., Boschetti, L., Abatzoglou, J. T., and Giglio, L.: Changes in fire activity in Africa from 2002 to 2016 and their potential drivers, *Geophysical research letters*, 46, 7643–7653, 2019.